Draft version 4.2

ATLAS NOTE

October 11, 2011

Search for new physics in a like-sign dimuon final state with ATLAS 2011 Data.

Juerg Beringer[a], Sourabh Dube[a], Andrei Gaponenko[a], Ian Hinchliffe[a], Michiru Kaneda[b]

[a]*Lawrence Berkeley National Laboratory*
[b]*CERN*

Abstract

We present preliminary results for a search for new physics in a like sign dimuon final state in proton-proton collisions at $\sqrt{s} = 7$ TeV. The data were collected with the ATLAS detector in 2011 at the LHC and correspond to an integrated luminosity of (1.31 ± 0.04) fb^{-1}. With a high track multiplicity requirement, we predict 56 ± 7 events from the Standard Model and we observe 60 events in the data. We interpret this result in the context of low-scale gravity models and set a limit on the cross section times acceptance for the production of mini blackholes.

Contents

1 Introduction

The hierarchy problem, in which the Planck scale ($M_{\rm Pl} = 1.2 \times 10^{19}$ GeV) is vastly large compared to the electroweak scale of 100 GeV, is one of the major motivations for new physics. A theory introducing extra dimensions is one possible solution. In some theories of extra dimensions, the gravitational field propagates into $n + 4$ dimensions, where n is the number of extra dimensions over the 4 spacetime dimensions. The Standard Model particles are localized in the 4 space-time dimensions. Since the gravitational field propagates into the extra dimensions, it is reduced from the fundamental gravitational force to the weak gravitational field we observe. Thus, the fundamental Planck scale in $n+4$ dimensions, $M_{\rm D}$, would be much smaller than $M_{\rm Pl}$ and comparable with the electroweak scale.

One of the theories of the extra dimensions is the ADD model, which is the model of large flat extra dimensions, proposed by Arkani-Hamed, Dimopoulos, and Dvali [1, 2, 3]. Extra dimensions are compactified in cylinder shape of which radius equal R, and $M_{\rm D}$ is related to $M_{\rm Pl}$ as [4, 5]

$$M_{\rm Pl}^2 = 8\pi R^n M_{\rm D}^{n+2}. \quad (1)$$

Experimental limits on $M_{\rm D}$ by the collider experiments are reported by the LEP and the Tevatron experiments; $M_{\rm D} > 1.60, 1.20, 1.04, 0.98, 0.94 , 0.80$ TeV for each $n = 2, \cdots, 7$, respectively [6, 7, 8]. The CMS experiment at the LHC excludes the production of black holes with $M_{\rm TH}$ of 4, 4.4, and 4.5 TeV for $M_{\rm D}$ of 1.5 TeV for $n = 2$, 4, and 6 respectively [9], where $M_{\rm TH}$ is the minimum mass of the produced black holes.

If extra dimensions exist and $M_{\rm D}$ is of order TeV, mini black holes with TeV scale mass can exist and they can be produced by the Large Hadron Collider. In this analysis, mini black holes were searched for in a same charge dimuon final state. The analysis presented in this note is an extension of the analysis carried out in 2010 data and documented in Ref. [10, 11]. The reader is urged to read those notes to gain an understanding of the motivation for this analysis and for some of the selections used here.

A brief review of the theoretical considerations of black hole production and decay can be found in [12].

1.1 Analysis Strategy

Black holes decay to all particles in the Standard Model. If black holes are produced with masses well above the new physics scale, they are anticipated to decay initially by Hawking evaporation. In this case, the relative production probabilities for different particle types from the black holes depend on the coupling of the particle to gravity, and the dynamics of the process given by the relative thermal emissivities. Since gravity couples only to the energy-momentum content of matter, it is anticipated that gravity couples to all particle degrees of freedom in the theory equally. The relative emissivity of the process is governed by the dynamics and depends on the mass, angular momentum, and gauges charges of the non-perturbative gravitation state and the mass, spin, and gauge charges of the particle being emitted.

The classic signature for a black hole decay is multiple high $p_{\rm T}$ objects. An analysis based on a multijet signature is presented in Ref. [13]. We use a different approach in this analysis: the signal region is defined in terms of *track* multiplicity, and we use leptons to reduce Standard Model backgrounds. Specifically, we require that there are two muons, and that the muons are of the same charge. This has the benefit of having very small Standard Model background, while having an appreciable signal acceptance. We perform a cut-and-count analysis after explicitly defining the signal selection in terms of track multiplicity.

1.1.1 Sources of Background

The muons from background processes considered in this analysis can come from three sources. Muons can arise from processes such as the decay of W (which are prompt muons - μ_{prompt}) and the semi-leptonic decay of b and c hadrons (HF muons - μ_{HF}). The decay in flight of pions and kaons also gives rise to muons, which we designate as non-prompt or fake muons (μ_{fake}). It is also possible to reconstruct muons from a pion or kaon which punches through to the muon spectrometer. For the following discussion and this analysis we include the punch throughs in μ_{fake} along with the decay-in-flight.

The backgrounds considered in this analysis fall in two categories. The two muons in an event can be produced in association, or they may be arise from decay chains with no connection to each other.

- Associated production of like sign dimuons consists of dimuons from the decay of $b\bar{b}$ [1] and $t\bar{t}$ events. These dimuon events are predominantly of the $\mu_{HF}\mu_{HF}$ category for $b\bar{b}$ and of the $\mu_{\text{prompt}}\mu_{HF}$ category for $t\bar{t}$. We estimate the $t\bar{t}$ background using a simulated sample. We estimate the $b\bar{b}$ background from simulated samples normalized to data as described in section 5.1.

- Like-sign dimuons from uncorrelated decay chains typically arise from W+jets events, where the leading muon is μ_{prompt} from W decay and the second muon is either a μ_{HF} from b, c decay or a μ_{fake} from the jets. Low energy QCD processes can also give like-sign dimuons. The dimuons in this case consist of the following categories : $\mu_{\text{prompt}}\mu_{HF}$, $\mu_{\text{prompt}}\mu_{\text{fake}}$, $\mu_{\text{fake}}\mu_{\text{fake}}$. To estimate this uncorrelated production we select all events with one muon and an extra track (or tracks). These events are weighted by the probability for a track (or tracks) to give rise to a muon to get the dimuon estimate. The measurement of this probability and the method is described in section 5.2.

2 Data Samples and Triggers Used

The data sample used for this analysis was collected with a single muon trigger with $p_{\text{T}} > 20$ GeV (EF_mu20). The data were processed with release 16 of the ATLAS software. The goodrun list produced by the SUSY Group [14] was used to select periods of data-taking suitable for this analysis. The integrated luminosity of the data sample is (1.31 ± 0.05) fb^{-1} [15].

3 Simulation Samples

The Monte-Carlo samples used in this analysis and their corresponding cross-sections are listed in Table 1. Some other details of the generated samples are shown in Table 8. The $t\bar{t}$ sample is generated with MC@NLO + JIMMY [16, 17, 18] at the nominal top mass of 172.5 GeVand is filtered to have one lepton (e or μ or τ with $p_{\text{T}} > 1$ GeV) at the generator level. The cross section for the $t\bar{t}$ process is taken from the top cross section paper [19]. The $t\bar{t}$ sample is generated using the CTEQ66 parton distribution function (PDF) [20].

The $b\bar{b}$ sample is generated with PYTHIA. It is filtered at the generator level to have two muons with $p_{\text{T}} > 10$ GeV each. The diboson samples (WZ and ZZ) are generated with HERWIG [21]. They are filtered to have at least one electron or muon with $p_{\text{T}} > 10$ GeV. The single top background in the Wt channel is estimated using a sample generated with ACERMC [22] [2]. The $b\bar{b}$, diboson and single top samples are all generated using the MRST2007 PDF [23].

The signal samples are generated with BLACKMAX [24, 25] and are hadronized with PYTHIA. The PDF used is the CTEQ66 PDF. The nominal black hole signal sample is for a rotating black hole with the

[1] The discussion of $b\bar{b}$ in this note implicitly includes dimuons from $c\bar{c}$ as well.

[2] The single top backgrounds from t and s-channel production are included in the data driven background estimate.

Process	Generator	Cross section (pb)	Luminosity(pb^{-1})
$b\bar{b} + c\bar{c}$	Pythia	2797	106.2
$t\bar{t}$	mc@nlo + Jimmy	164.6	120.6×10^3
ZZ	Herwig	6	197.6×10^3
WZ	Herwig	18	45.1×10^3
Wt	AcerMC	14.6	20.5×10^3
BH M_{TH} = 4 TeV, M_D = 0.8 TeV, n = 6	Blackmax	2	9.6×10^3

Table 1: Monte Carlo samples used for background estimates in this analysis. The cross section for $t\bar{t}$ is from the top paper [19], and for the single-top Wt is from the single-top note [27]. The cross sections for the other processes are obtained from Ref. [28].

following parameters: M_D = 800 GeV, M_{TH} = 4000 GeV, 6 extra dimensions. The cross section for this point is 2 pb.

All simulation samples are generated with the pileup conditions corresponding to MC10b [26].

4 Event Selection

The basic event selection is two muons of the same charge. We describe the details of this selection below.

- Data events are required to pass the EF_mu20 trigger. No trigger requirement is imposed on MC events.
- We require a primary vertex with the number of tracks associated to the vertex > 5. The tracks in this case are required to have $p_T > 150$ MeV.
- Combined muons are selected from the StacoMuonCollection [29]. The muons are required to have $|\eta| < 2.4$ and pass the tight muon criteria as defined by the muon performance group. In addition the muon track should have a B-layer hit if the track traverses an active B-layer module, at least one hit in the pixel detector, at least 6 hits in the SCT, and pass TRT requirements recommended by the MCP group. The muons are required to come from the primary vertex by calculating the muon track z_0 with respect to the primary vertex and requiring that $|z_0 \sin(\theta)| < 1.5$ mm. This is done to ensure that even in high pile-up events, the muons and the selected tracks in the signal region (as describe below) will come from the primary interaction.
- The muons are ordered in p_T. The leading muon is required to have $p_T > 25$ GeV, and the second muon is required to have $p_T > 15$ GeV.
- The leading muon is also required to be isolated by requiring the sum of transverse momenta of tracks in a cone of $\Delta R_{\eta-\phi} < 0.2$ around the muon (ptcone20) to be less than $0.2\times p_T$ of the muon.
- The leading muon is required to have low impact parameter significance by imposing $|d_0/d_0^{err}| < 3$. The impact parameter is calculated with respect to the primary vertex in the event.
- No isolation or impact parameter requirements are made on the second muon. Muons can arise promptly from the black hole, or from the decay of heavy flavor quarks from the black hole. By not requiring isolation, good signal acceptance to these heavy flavor muons is maintained.

- The muons are required to satisfy $\Delta R_{\eta-\phi} > 0.2$ to explicitly ensure that the isolated muon is away from the second muon.

- The leading and second muons are required to have the same charge.

- The tracks used in the counting of track multiplicity (NTracks) are required to have $p_T > 10$ GeV. Tracks are also required to have $|\eta| < 2.4$, and pass all the same inner detector hit requirements as the muons. The tracks are also required to come from the primary vertex by requiring that $|z_0 \sin(\theta)| < 1.5$ mm. The track count includes the two muons.

The track multiplicity, NTracks, is used to define two regions. A background region with NTracks < 10 and the signal region with NTracks ≥ 10. The background region has identical requirements except for the inverted NTracks selection. Appendix A shows the p_T and NTrack distributions for sample signal models.

4.1 Muon Trigger and Identification

No trigger requirement is imposed on MC events. Instead the MC events are weighted according to their probability of being triggered by any muon in the event. The weight is computed using the efficiency curves from Ref. [30]. The trigger efficiency has been measured in data for good offline Staco muons which match to the trigger at L1 within $\Delta R_{\eta-\phi}$ of 0.5. We make this same requirement in our data events for consistency. The trigger efficiency for EF_mu20 is at a plateau for $p_T > 20$ GeV and the plateau efficiency is 75% for muons in the barrel and 88% for muons in the endcap. In the analysis we use p_T dependent trigger efficiencies for endcap and barrel, which are measured for three different run ranges, 178044≤ Run ≤182519 (75% plateau for barrel), 182519< Run ≤183347 (72% plateau for barrel) and Run >183347 (77% plateau for barrel). The efficiency in the endcap is the same (88% plateau) for all run ranges.

The MC predicts the muon identification and reconstruction efficiencies very well. As per the recommendations of the Muon Combined Performance Group [29], we apply weights to the MC events which are dependent on muon η and ϕ to account for the differences in muon identification efficiency in data and MC. We also smear the muon p_T according to the recommendations. The MC samples are reweighted to match their $< \mu >$ distribution to data, where $< \mu >$ is the mean number of interactions in an event.

5 Background Estimation

We group possible sources of background into the following two categories:

- Processes with associated production of dimuon events of the same sign. These include $b\bar{b}$, $t\bar{t}$, diboson (WZ,ZZ) production as well as single top production in the Wt channel (which is identical to $t\bar{t}$). The backgrounds from $t\bar{t}$, single-top and dibosons are estimated completely from simulation using samples listed in Table 1. In the signal region, the diboson and single-top backgrounds are found to be negligible. The $b\bar{b}$ background is estimated using data and simulation as described in section 5.1. The dominant background in this category is $t\bar{t}$.

- Processes with same-sign dimuons, where the muons come from uncorrelated decay chains. We expect the dominant process to be W+jets where one muon comes from W decay and the other muon comes from a pion/kaon decay in flight or the semi-leptonic decay of b, c hadrons. We estimate this contribution completely from data by measuring the probability of a track to give a muon, and applying this to all muon+track events in the signal region. The method is further

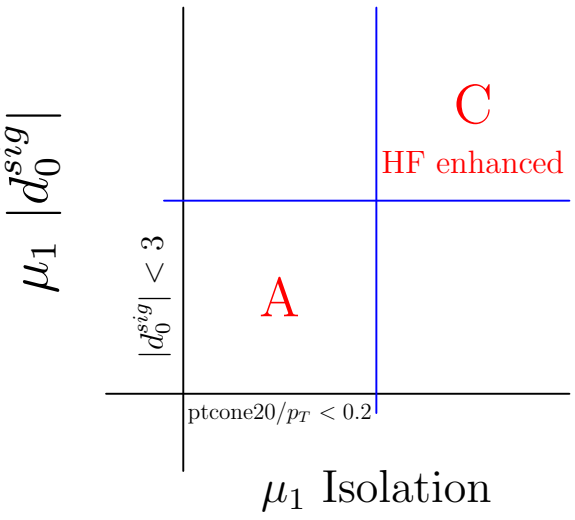

Figure 1: Figure shows a schematic of the different kinematic regions used for $b\bar{b}$ estimation. The phase space is divided into regions based on d_0 significance and isolation of the leading muon. The signal region is A, with isolated leading muon with low impact parameter significance. Region C has additional selections to enhance the heavy-flavor fraction.

explained in section 5.2. This background will include contributions from Z+jets, and single-top in the t and s channels, along with low-p_{T} QCD.

5.1 Estimation of $b\bar{b}$ background

The $b\bar{b}$ background is estimated by using a heavy-flavor rich control region in data and extrapolating to the signal region using the $b\bar{b}$ MC sample. The estimate is obtained in two steps. In the first step, the kinematic regions shown in Fig. 1 and described below are used to obtain a $b\bar{b}$ estimate in the background region with NTracks < 10. In the second step, the $b\bar{b}$ MC is used to extrapolate the prediction from the background region to the signal region (NTracks ≥ 10). The steps are described below.

5.1.1 Step 1 - In the background region with NTracks < 10

Figure 1 shows the relevant kinematic regions.

Region A is the region of interest; the leading muon has ptcone20/$p_{\mathrm{T}} < 0.2$ and $|d_0^{sig}| < 3$. Let us denote by A_{data} the number of $b\bar{b}$ events in region A in data, with A_{MC} denoting the number of events from $b\bar{b}$ MC. Region C has inverted requirements on the isolation and d_0^{sig} of the leading muon. In addition, the leading and second muon in region C must satisfy $1 - p_{\mathrm{T}}^{MS}/p_{\mathrm{T}}^{ID} < 0.2$ to enhance the heavy flavor fraction (see Appendix C). Let C_{data} and C_{MC} denote the number of events in region C in data and $b\bar{b}$ MC respectively.

We measure the ratio $R = A_{MC}/C_{MC}$ in the $b\bar{b}$ MC. The ratio is $0.328 \pm 0.028(stat)$. A_{data} is then given by $R \cdot C_{data}$. Mathematically, this is identical to the method used in Ref. [10]. In data, $C_{data} = 6480$ events. In addition we model the shapes of the muon p_{T} and $E_{\mathrm{T}}^{\mathrm{miss}}$ distributions in region A_{data} using the shapes in C_{data}. By using the shapes from C_{data} we are able to ameliorate several issues. C_{data} has higher statistics than A_{data} and thus lower statistical uncertainties, unlike the MC. C_{data} is also naturally better to model pile-up effects of the data.

For the method to work, the distributions of d_0 significance and isolation are required to be well modeled in the simulation. In Fig. 2 we show the d_0 significance for the leading muon in region C. In

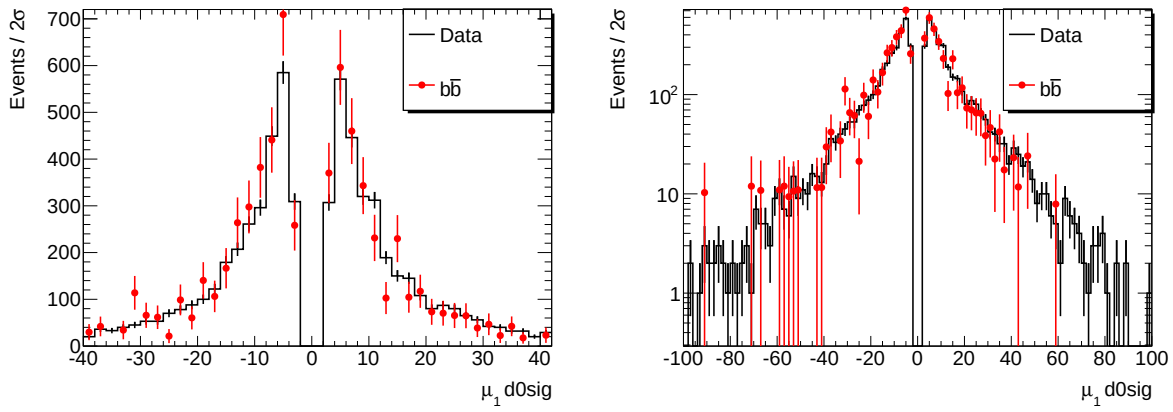

Figure 2: Figure shows the d_0/d_0^{err} distribution for the leading muon in region C, in events where the leading muon has ptcone20/$p_{\mathrm{T}} > 0.2$. The distributions are normalized to area. The KS probability of the agreement of shapes is 0.11. The figure on the left is with a linear scale on y-axis, the right is with a log scale.

Fig. 3 we show the d_0 significance and isolation for the second muon in region C. While we make no requirements on d_0 significance and isolation for the second muon, the agreement shown in the figure gives confidence in the modeling of these variables in the simulation. Region C is expected to be dominated by $b\bar{b} + c\bar{c}$, with total contributions of $t\bar{t}$ and W+jets estimated from MC to be around 2% of the total. The comparison of the shapes of the p_{T} and $E_{\mathrm{T}}^{\mathrm{miss}}$ distributions between C_{data} and A_{MC} is shown in Fig. 4. These show good agreement; the KS probability for the agreement of shapes ranges from 0.11 for the leading muon d_0 significance distribution to 0.59 for the leading muon p_{T} distribution.

5.1.2 Step 2 - Extrapolating to signal region (NTracks $\geq$ 10)

The region C_{data} cannot be used with NTracks $\geq$ 10 due to potential signal in this region. The signal region has zero events in the $b\bar{b}$ MC. To estimate the fraction of $b\bar{b}$ events in the signal region, the NTracks shape in the $b\bar{b}$ MC, i.e. in A_{MC} is extrapolated into the signal region. A simple exponential function is used for the fit to NTracks and the fit is shown in Fig. 6 (left). The fitted function is Events= $e^{a-b\times\mathrm{NTracks}}$, with $a = 6.5 \pm 0.2$, and $b = 0.94 \pm 0.08$. The function is then integrated from 10 to infinity to obtain the total number of events with NTracks $\geq$ 10. The ratio of events in the signal region to the background region is 0.00036. This ratio, and A_{data} calculated above yields the $b\bar{b}$ background in the signal region as 0.77 events. We assign a 100% systematic uncertainty to the $b\bar{b}$ prediction as a conservative choice.

A cross check of this method is done by relaxing the p_{T} requirements on the two muons in the $b\bar{b}$ MC till one event is found in the signal region. The relaxed cuts are $p_{\mathrm{T}} > 12, 11$ GeV for the two muons. The ratio of events in signal region to the background region in this relaxed sample is 0.00031 with a 100% uncertainty.

The nominal fit is done using all events in the $b\bar{b}$ sample, i.e. for 2 < NTracks < 8. We also try various fit ranges such as [2 − 5] (predict: 0.65), [3 − 8] (predict: 1.1) and [4 − 8] (predict: 1.9). The various predictions are in decent agreement with the nominal prediction of 0.77 given the 100% uncertainty.

We check the choice of fit, and perform a closure test of the method in the $t\bar{t}$ MC. This is shown in Fig. 6 (right). The NTracks distribution has a different shape for NTracks < 5 in $t\bar{t}$ versus $b\bar{b}$ as the $t\bar{t}$ process peaks at 4 tracks (two W's and two b's in each event). We fit the NTracks for 6 <NTracks< 11. We then use the fit to predict the number of events with NTracks $\geq$ 15 and $\geq$ 20. The predicted number

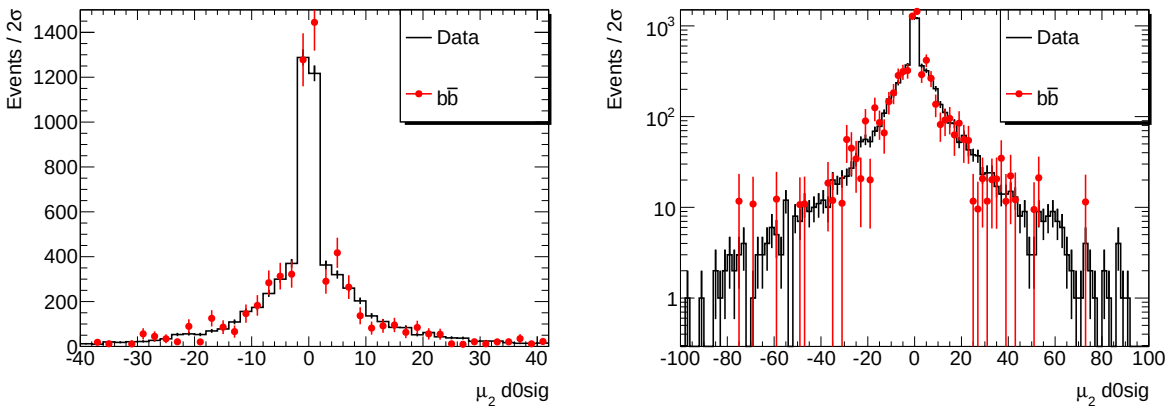

(a) Region C : μ_2 d_0/d_0^{err} distribution.

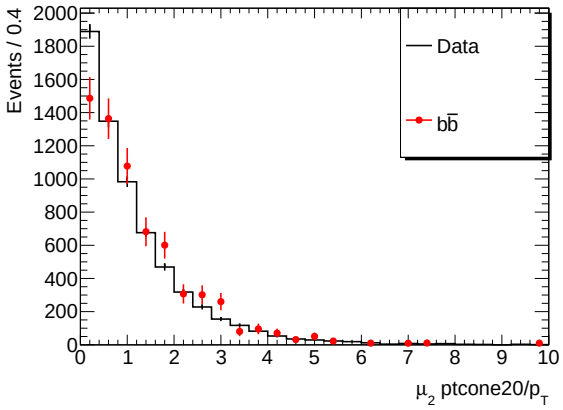

(b) Region C: μ_2 isolation distribution.

Figure 3: Figure shows the d_0 significance (3(a)) and isolation(3(b)) distributions for the second muon for events in region C. The data distribution has been normalized to the simulation. The KS probability of the agreement of shapes is 0.64 for the d_0 significance distribution, and 0.03 for the isolation distribution. Although no selections are made on the second muon, these distributions give confidence in the modeling of the distributions in MC. See section 5.1.1 for details.

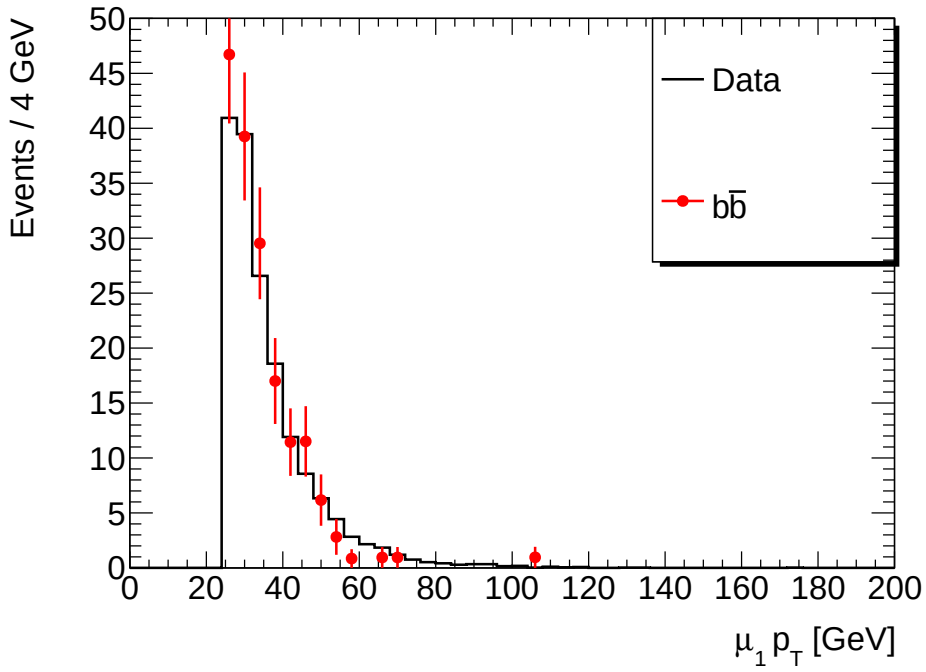

(a) Region A, C : p_{T} distribution.

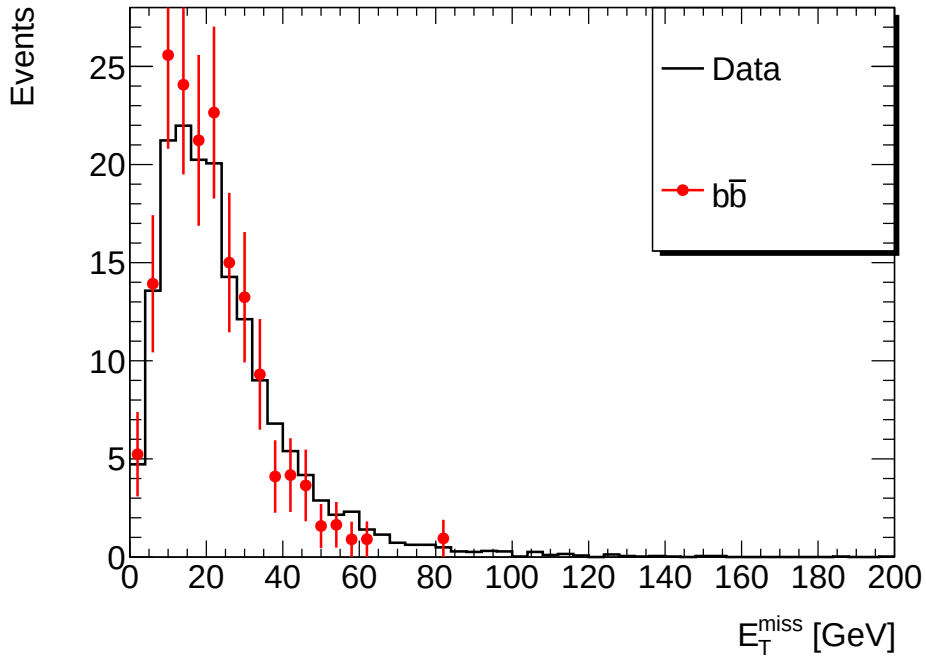

(b) Region A, C: $E_{\mathrm{T}}^{\mathrm{miss}}$ distribution.

Figure 4: Figure shows the p_{T} distribution for the leading muon (4(a)) and $E_{\mathrm{T}}^{\mathrm{miss}}$ distribution(4(b)) for events in regions C_{data} and A_{MC}. The data distribution has been normalized to the simulation. The KS probability of the agreement of shapes is 0.59 for the p_{T} distribution and 0.21 for the $E_{\mathrm{T}}^{\mathrm{miss}}$ distribution. See section 5.1.1 for details.

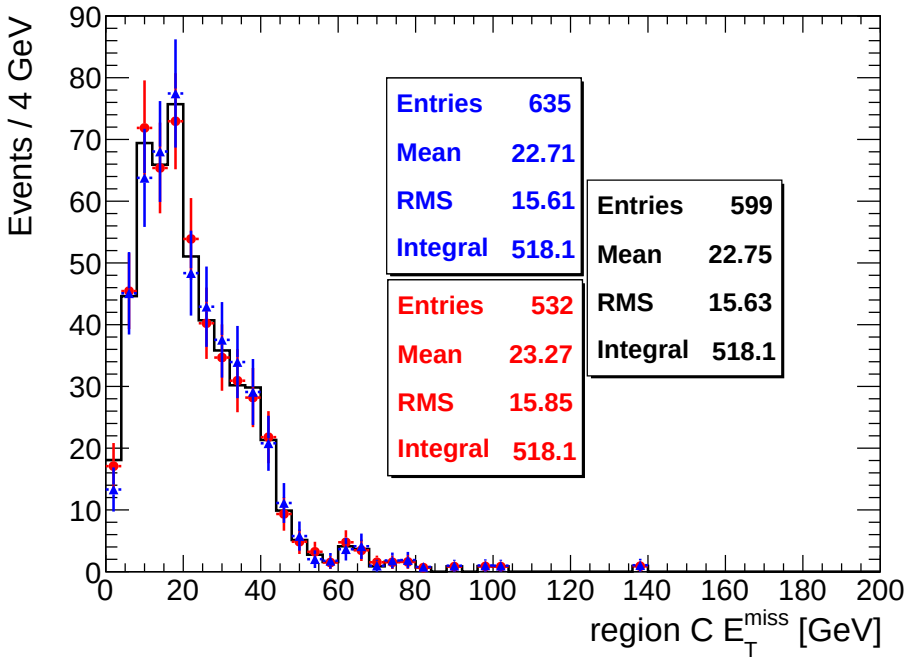

(a) Region C : $E_{\mathrm{T}}^{\mathrm{miss}}$ distribution.

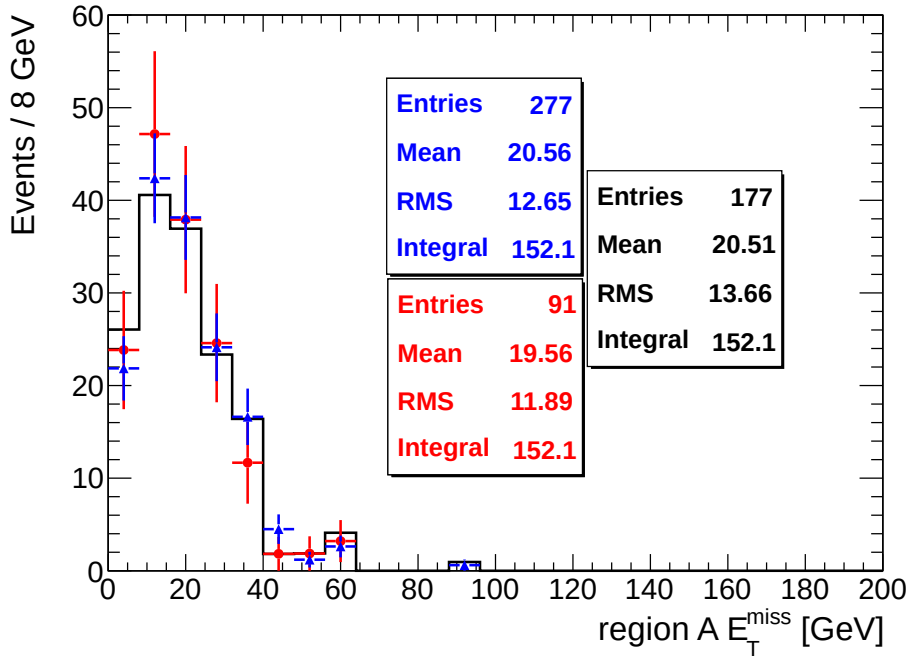

(b) Region A: $E_{\mathrm{T}}^{\mathrm{miss}}$ distribution.

Figure 5: Figure shows the $E_{\mathrm{T}}^{\mathrm{miss}}$ distribution in region C (5(a)) and region A (5(b)) for three different choices of muon isolation in the $b\bar{b}$ MC. The black solid line shows the nominal isolation requirement ptcone20/p_{T} < 0.2, the red circles are with ptcone20/p_{T} < 0.3, the blue triangles are with ptcone20/p_{T} < 0.1. The distributions with higher and lower isolations are normalized to the distribution with nominal isolation. The shape of the $E_{\mathrm{T}}^{\mathrm{miss}}$ is same in all cases implying that it is uncorrelated with the choice of the isolation requirement.

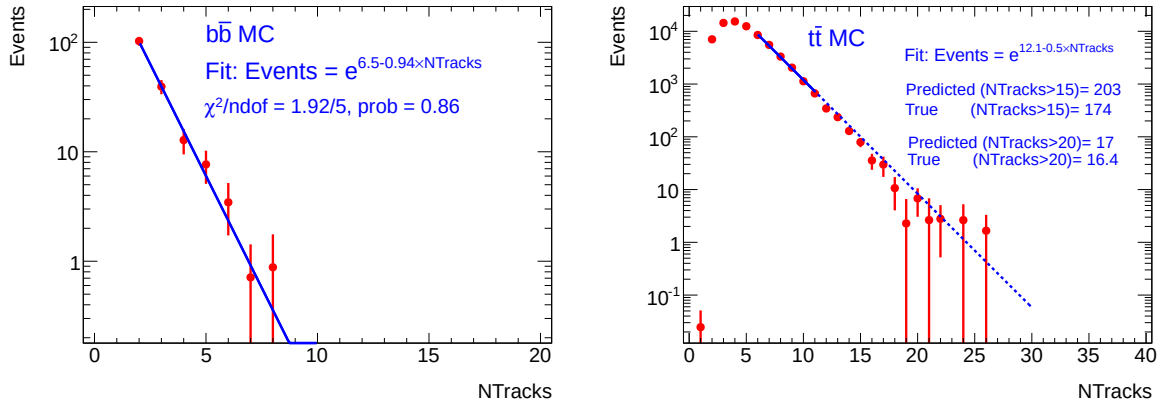

Figure 6: Figure shows the NTracks distribution for $b\bar{b}$ (left) and $t\bar{t}$ (right) simulation for like-sign dimuon events. See section 5.1.2 for details.

of events for NTracks $\geq$ 15 from the fit is 203, and the true number of events is 174. For NTracks $\geq$ 20 we predict 17 events and the true number of events is 16.4. If we fit the distribution for 5 <NTracks< 10, we predict 28 events for NTracks $\geq$ 20. The prediction and truth agree well within the 100% uncertainty that we assign. We consider this a successful closure test.

5.2 Data based estimate of the fake background

In this section, we describe a data driven measurement of the fake muon background as it applies to this analysis. The procedure consists of two steps: first we measure the *per-track* fake rate on a control sample of events in data. We then apply this rate to data events with one muon + one or more tracks where the muon passes the requirements of the leading muon for the analysis. This gives us a prediction for dimuon events. While this method includes the contributions from Z+jets, and QCD dijet processes, in practice the background is dominated by the W+jets process.

For the control sample we use W+track events. We select events with $25 < E_{\mathrm{T}}^{\mathrm{miss}}(\mathrm{GeV}) < 80$ and one isolated muon with $p_{\mathrm{T}} > 25$ GeV. We form the transverse mass (m_{T}) of the muon with $E_{\mathrm{T}}^{\mathrm{miss}}$ and require that $50 < m_{\mathrm{T}}(\mathrm{GeV}) < 120$. We also require NTracks < 10 to remove signal contribution. In these selected W events, we require an additional track with $p_{\mathrm{T}} > 15$ GeV, which passes the tracking requirements as listed in section 4. The track is required to have the same charge as the muon. This forms the denominator. Each eligible track in the event is used for the denominator.

For the numerator, we require that an additional muon with $p_{\mathrm{T}} > 15$ GeV exists in the event passing all muon requirements and this additional muon is of the same charge as the muon. The muon is also matched to a denominator track. The numerator and denominator give us the rate of obtaining a second muon of the same charge given a track. We measure this rate as a function of the track p_{T}. In events with more than one additional muon satisfying the requirements, all possible muons enter the numerator.

To avoid double counting we subtract the contributions of $b\bar{b}$, $t\bar{t}$, Wt and dibosons ($WZ + ZZ$) to the fake rate by using the MC-driven methods that were discussed earlier in this section. The subtraction is done from the fake rate in bins of track p_{T} or η. In Fig. 7 we show the numerator as measured in the data before the subtraction, and the estimates of the contributions which will be subtracted.

Figure 8 shows the measured fake rate as a function of track p_{T} and $|\eta|$ [3]. The fake rate is constant for $p_{\mathrm{T}} > 20$ GeV. We measure the fake rate in two bins, one for $p_{\mathrm{T}} < 20$ GeV and one for $p_{\mathrm{T}} > 20$ GeV. The fake rate (and error) for $p_{\mathrm{T}} > 20$ GeV is obtained by fitting the fake rate with a straight line. For

[3] The p_{T} fake rate is shown integrated for all η, and vice versa

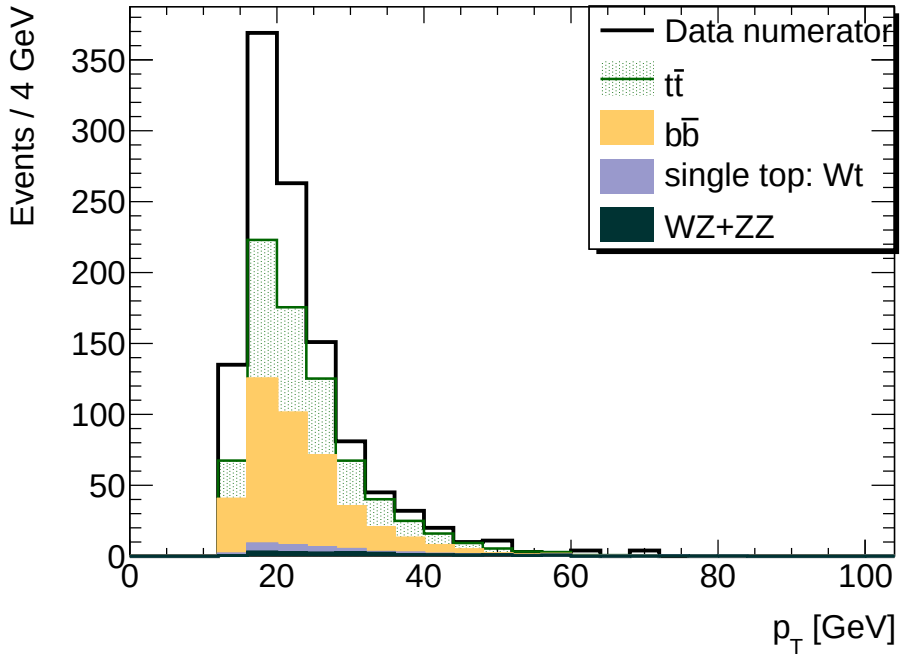

Figure 7: Figure shows the p_{T} distribution of the numerator in data before any subtractions. The contributions to this numerator from $b\bar{b}$, $t\bar{t}$, Wt and diboson ($WZ + ZZ$) production are also shown as stacked histograms. These will be subtracted from the data before the fake rate is measured.

Track p_{T} [GeV]	Fake Rate
$15 < p_{\mathrm{T}} < 20$	0.0044 ± 0.00015
$20 < p_{\mathrm{T}} < 60$	0.0037 ± 0.00012
$p_{\mathrm{T}} > 60$	0.0037 ± 0.0021

Table 2: The measured fake rate and uncertainties in the different p_{T} bins.

$p_{\mathrm{T}} > 60$ GeV, the error on the fake rate is taken from the $60 < p_{\mathrm{T}}[\text{ GeV}] < 120$ bin shown in Fig. 8. The measured fake rate and uncertainties are shown in Table 2. The constant fake rate for $p_{\mathrm{T}} > 20$ GeV is motivated by MC studies (see Appendix D).

The fake rate increases slightly with increasing $|\eta|$. The effect of averaging over the central η hole ($|\eta| < 0.1$) is studied by measuring the p_{T} dependent fake rate separately for $|\eta| < 0.1$ and $|\eta| > 0.1$. However, this shows no change in the final predictions. The final fake rate is averaged over all η for simplicity.

To estimate the background, we select a sample of muon+track events in data, where the muon passes the requirements of the leading muon for the analysis and the track passes the same requirements as above. If more than one track passes the cuts, each of them is considered. We compute the probability for an event to contain a fake and apply it as an event weight. For an event with n tracks, this probability is $(1 - \prod_{i=1}^{n}(1 - p_i))$, where p_i is the probability for the i^{th} track to fake a muon.

By design, the contribution of double-fakes is included since the selection of muon+track events will include events where the leading muon is a fake.

A validation of this procedure in simulation samples has been presented in Ref. [10].

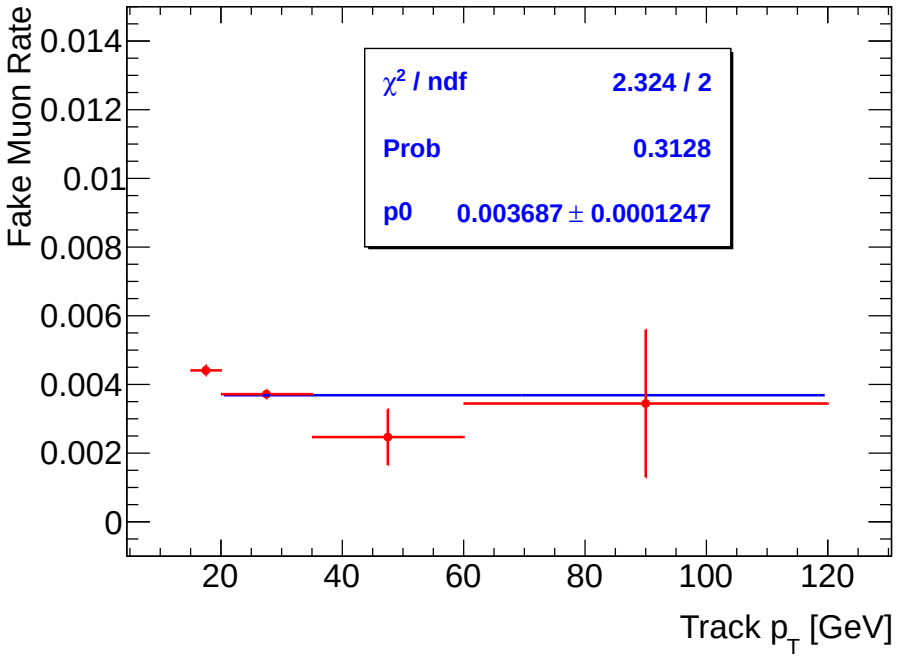

(a) Fake rate as function of p_{T}.

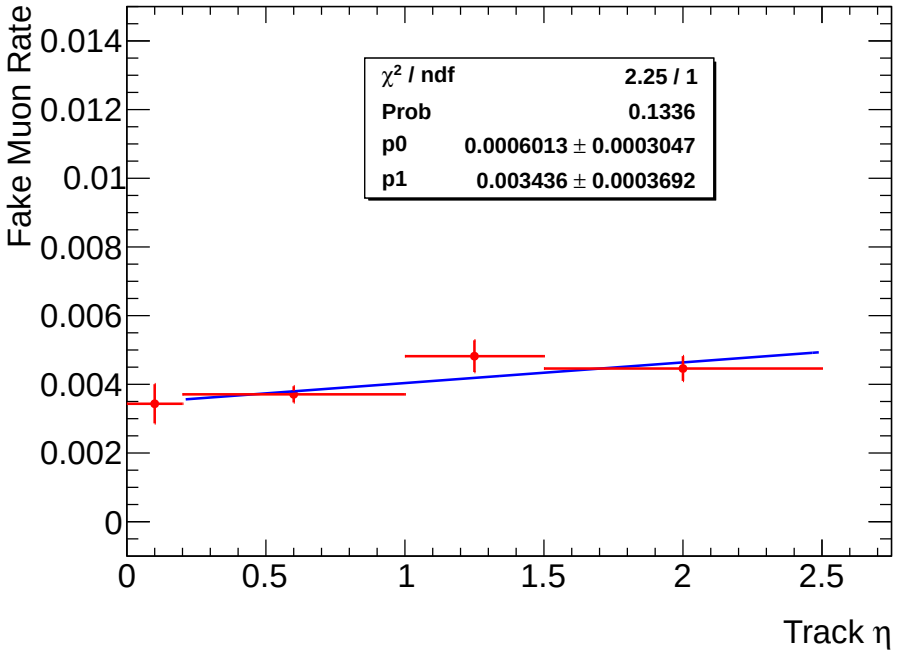

(b) Fake rate as function of $|\eta|$.

Figure 8: Figure shows the measured fake rate in data as a function of track p_{T} (8(a)) and η (8(b)).

Process	Events
$b\bar{b}$	2125 ± 26(stat) ± 181(syst)
$t\bar{t}$	748 ± 2(stat) ± 104(syst) ± 28(lumi)
μ+fake	1304 ± 2(stat) ± 261(syst)
Wt	53.2 ± 1.7(stat)
$WZ + ZZ$	35.7 ± 0.9(stat)
Predicted	4266 ± 26(stat) ± 335(syst)
Observed	3775

Table 3: Number of expected and observed events in the low NTracks control region. The systematic uncertainties are discussed in section 6. The systematic uncertainties on the diboson ($WZ + ZZ$) and single-top (Wt) backgrounds are not evaluated.

5.3 Validation of Background Estimate

We validate the various background estimation techniques in data by predicting the number of events with NTracks < 10. The complete selection is as described in section 4.

Table 3 shows the expected and observed events in this control region. For the $b\bar{b}$ background, only the uncertainty on the ratio $R = A_{MC}/C_{MC}$ as shown in section 5.1 is included. The systematic uncertainties on the diboson and single-top backgrounds are not evaluated as they are expected to be negligible compared to the dominant backgrounds. Figure 9 and Fig. 10 show the p_{T} distributions for the leading and second muons respectively. Figure 11 shows the dimuon invariant mass distribution. The corresponding figures with the ratio of data to background are shown in Figures 37, 38, and 39.

5.3.1 Validation of $t\bar{t}$ MC

The $t\bar{t}$ MC prediction is validated in a control region with the following selection.

- Events are required to have two opposite-sign muons with $p_{\mathrm{T}} > 25, 15$ GeV respectively. The muons are required to be isolated by requiring ptcone20/$p_{\mathrm{T}} < 0.2$ for both.
- A third muon (of either charge) with $p_{\mathrm{T}} > 15$ GeV is required. No isolation is imposed on the third muon.
- Events are required to have high missing energy; $E_{\mathrm{T}}^{\mathrm{miss}} > 60$ GeV.
- Events are required to have NTracks < 10 to remove potential signal contamination.

With this selection, $t\bar{t}$ production is dominant. The predicted number of events, and the data observation is shown in Table 4. The $\mu\mu$+fake contribution is estimated in the same way as the $\mu + fake$ background estimate discussed in section 5.2, and is dominated by the Z+jets process. The other predictions (viz. $t\bar{t}$, WZ, ZZ) are made using the nominal simulation samples. The observed number of events in data agrees with the prediction at the 20% level, and the prediction of the $t\bar{t}$ MC sample is thus validated.

6 Systematic Uncertainties

6.1 Data based estimation of background

The uncertainty on the muon fake rate due to measurement statistics is 8%. The rate is applied to each track in muon+track events. Let the rate be denoted by f_i for the i^{th} track. When events have more than

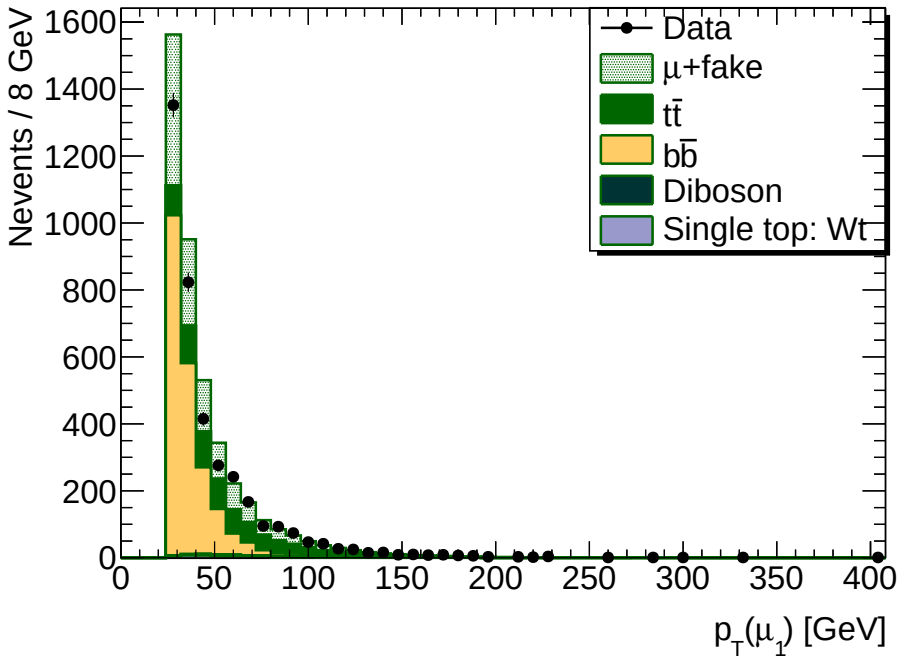

(a) Leading muon p_T: NTracks < 10

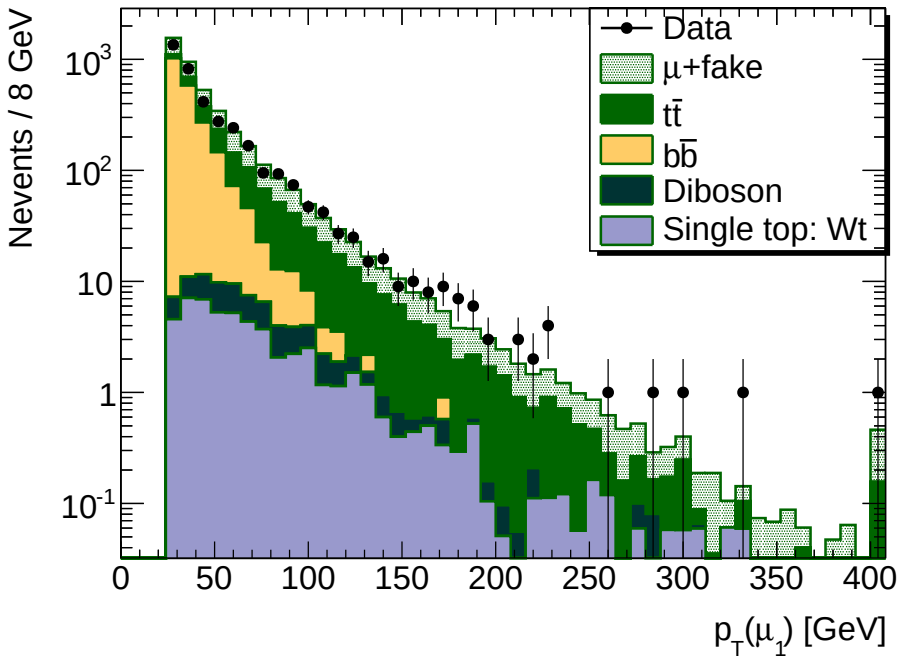

(b) Leading muon p_T: NTracks < 10

Figure 9: The leading muon p_T distribution in linear and log scale in the background region. The background histograms are stacked. The rightmost bin along X-axis shows the overflows.

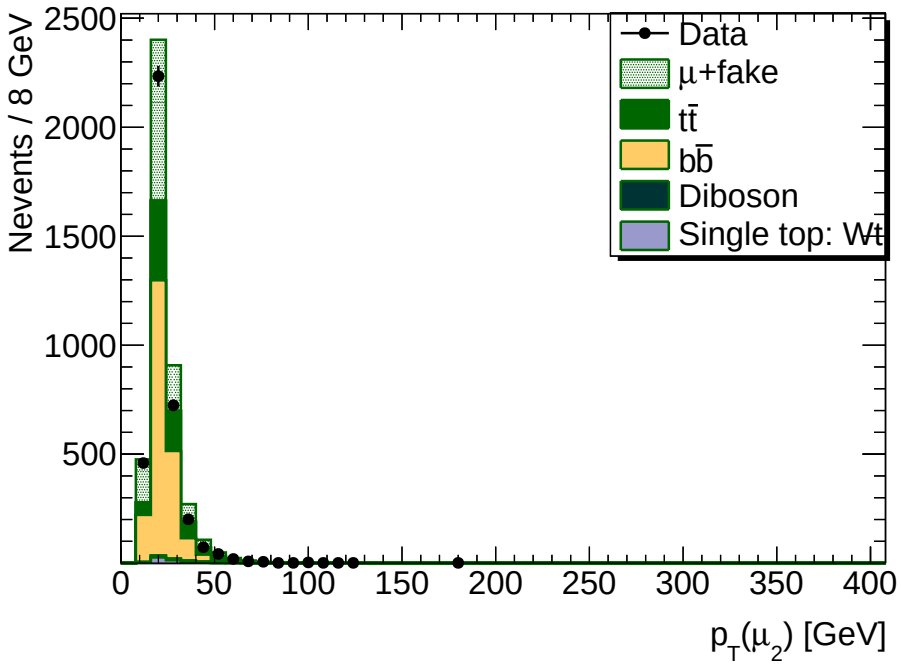

(a) Second muon p_T: NTracks < 10

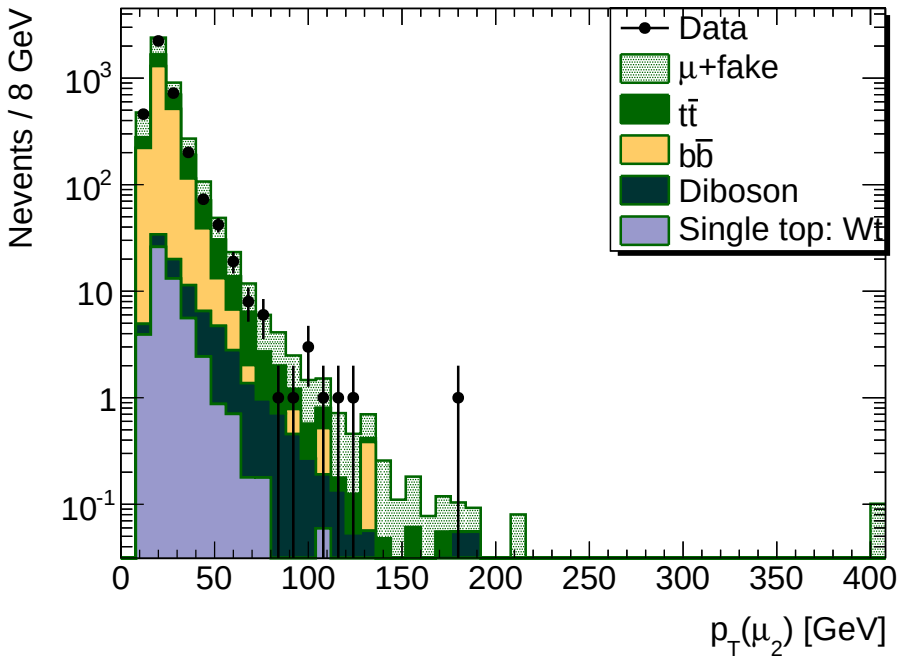

(b) Second muon p_T: NTracks < 10

Figure 10: The second muon p_T distribution in linear and log scale in the background region. The background histograms are stacked. The rightmost bin along X-axis shows the overflows.

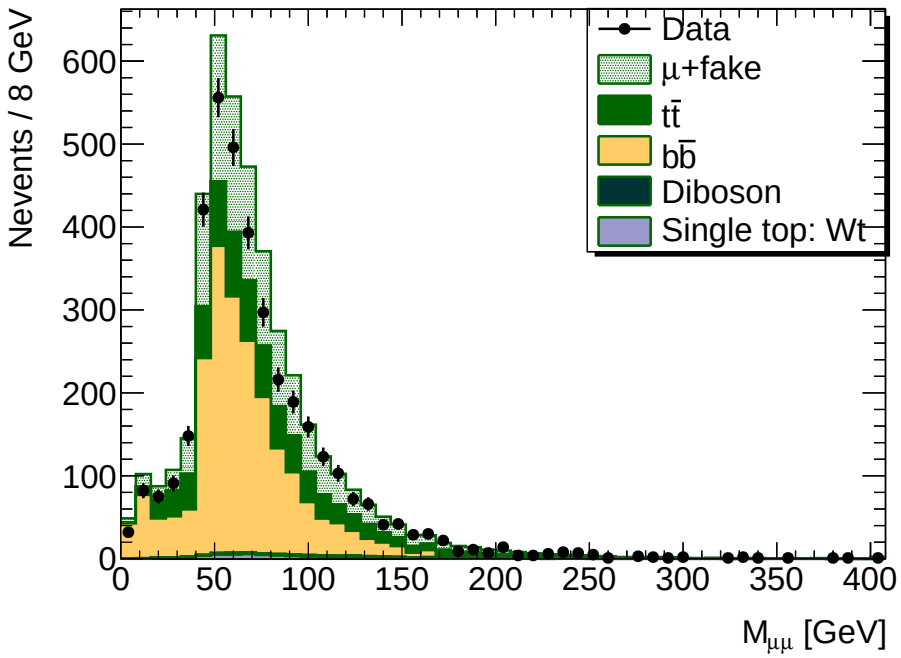

(a) Dimuon Invariant Mass: NTracks < 10

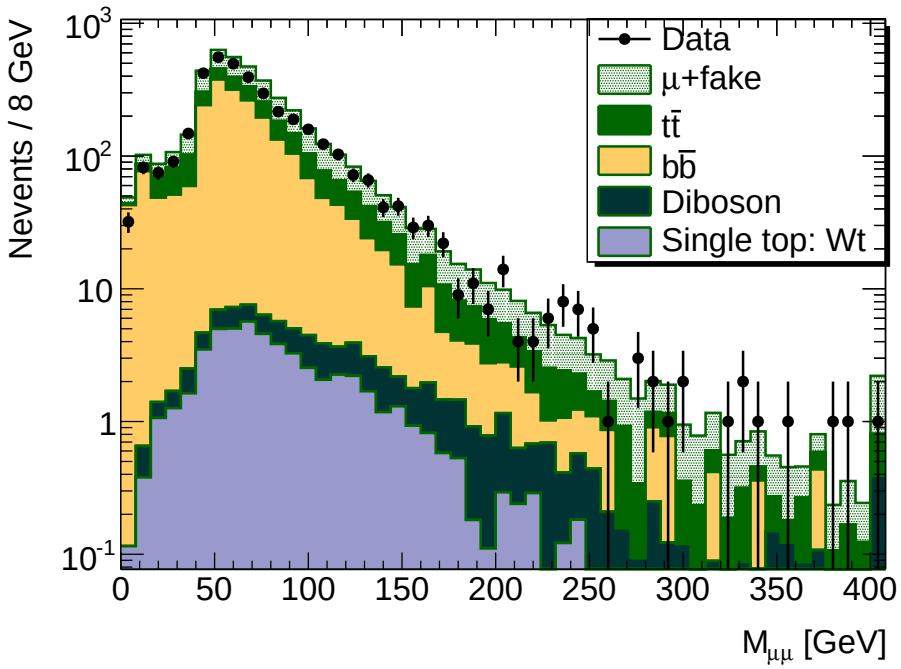

(b) Dimuon Invariant Mass: NTracks < 10

Figure 11: The invariant mass distribution of the two muons in linear and log scale in the background region. The background histograms are stacked. The rightmost bin along X-axis shows the overflows.

Process	Events
$t\bar{t}$	41.4 ± 0.6(stat) ± 6.0(syst) ± 1.5(lumi)
$\mu\mu$+fake	5.8 ± 0.1(stat) ± 1.2(syst)
$WZ + ZZ$	7.9 ± 0.4(stat)
Wt	2.3 ± 0.4(stat)
Predicted	57.4 ± 0.8(stat) ± 6.1(syst)
Observed	78

Table 4: Number of expected and observed events in the $t\bar{t}$ control region. Systematic uncertainties on the backgrounds from dibosons and Wt are not considered.

one eligible track, the total event weight is given by $w = 1 - \prod_{i=1}^{n}(1 - f_i)$. The uncertainties on f_i for all tracks in a given event are completely correlated and we account for this correlation when calculating the uncertainty on w. The sum of uncertainties for all such events gives the uncertainty on the data based estimate of background from the measurement statistics.

Some other effects that we considered are described here.

- The nominal fake rate is measured after subtracting $b\bar{b}$ and $t\bar{t}$ contributions as shown in Fig. 7. The total subtraction ($t\bar{t} + b\bar{b}$) is varied up and down by 1σ to get a low and high fake rate respectively. The $t\bar{t}$ background is varied by the total systematic uncertainty on this background (see Table 5). The $b\bar{b}$ background is varied by the uncertainty on R (see sec 5.1.1). The difference in background predictions from the low and high fake rate is -20% and $+18\%$. We take a systematic uncertainty of 20% on the μ+fake background due to this subtraction.

- The selection of W events is a possible source of systematic uncertainty. To estimate this, we perform the same measurement in a Z window. We select dimuon events of opposite sign which satisfy an invariant mass requirement ($76 < M_{\mu\mu} < 106$ GeV). Both muons are required to be isolated. In these dimuon events, we look for an extra track to form the denominator. Then we look for a third muon in the event passing all muon requirements for the second muon of our analysis. This forms the numerator. We compare the muon rate from the W-window and Z-window integrated over all track p_{T}. The rate from W after $b\bar{b}$, $t\bar{t}$ and diboson subtraction is $0.0033 \pm 0.0002(stat) \pm 0.0007(syst)$. The corresponding rate from Z is $0.0043 \pm 0.0004(stat)$. These rates are in reasonable agreement and we do not assign a systematic uncertainty for W-window selection.

The total systematic uncertainty on the data based estimate is thus a sum in quadrature of the uncertainty from measurement statistics and the 20% due to subtraction of other processes.

6.2 Estimation of $t\bar{t}$ background

The $t\bar{t}$ background is estimated using MC samples. The uncertainty on the theoretical cross section of $t\bar{t}$ is 9.6% [31, 32]. Predictions in Ref. [32] are calculated with Hathor [33] with $m_{\mathrm{top}} = 172.5$ GeV, and CTEQ66. The uncertainty is calculated by adding the scale and PDF uncertainties linearly. The scale uncertainty is 5.6%, while the PDF uncertainty is 4%. We consider the following systematic variations :

- To check the effect of generator we check the $t\bar{t}$ background from samples generated with POWHEG and hadronized with either JIMMY or PYTHIA. This yields a 5.1% uncertainty in the signal region.

- We also vary the mass of the top quark down to 170 GeV and up to 175 GeV. This yields a 4.5% systematic in the signal region.

Source	Muon+fake (%)	$t\bar{t}$ (%)	b/c (%)	Signal (%)
Measurement statistics	4			
Subtraction of $t\bar{t} + b/c + Wt$+diboson	20			
ISR/FSR		7		
t-quark mass		4.5		
Cross section		$^{+7}_{-9.6}$		
Generator		5.1		
Luminosity		3.7		3.7
μ reco/trig		2.6		1.5
PDF(Acceptance)				3
Rescale Truth Acceptance				14
Ratio (nominal/inverted)			8.5	
Extrapolation to NTracks ≥ 10			100	
Total uncertainty	20.4	14.4	100	15

Table 5: Systematic uncertainties in percent on the background estimates in the signal region from various sources. μ reco/trig stands for the uncertainty due to trigger efficiency weight and muon reconstruction efficiency scale factors applied to the Monte Carlo events.

- We test the effect of initial and final state radiation by checking the $t\bar{t}$ prediction using a sample where the ISR and FSR have been enhanced over nominal versus a sample where both ISR and FSR have been decreased versus nominal. These samples have been generated with ACERMC and hadronized with PYTHIA. This yields an uncertainty of 7%.

- The systematic uncertainty due to trigger efficiency and muon identification scalefactors is 2.6%.

The total systematic uncertainty on $t\bar{t}$ from all sources is 14.5%.

6.3 Estimation of $b\bar{b}$ background

In the background region with NTracks < 10, the uncertainty on $b\bar{b}$ background is from the measurement of $R = A_{MC}/C_{MC}$ as described in section 5.1. In the signal region, in addition a 100% uncertainty is taken on the $b\bar{b}$ estimate which arises from the extrapolation in the NTracks variable as described in Step 2 in section 5.1.

7 Results

Table 6 shows the expected and observed number of events for like-sign dimuon events with NTracks ≥ 10. The expected background contributions from diboson and single-top Wt are listed as other backgrounds. In Table 7, the prediction and observation is shown broken into categories based on muon charge.

Figure 12 shows the NTracks distribution for signal and background control regions. Figure 13 shows the p_{T} distributions of the leading and second muon in the signal region. Figure 14 shows the invariant mass distribution of the dimuons in the signal region.

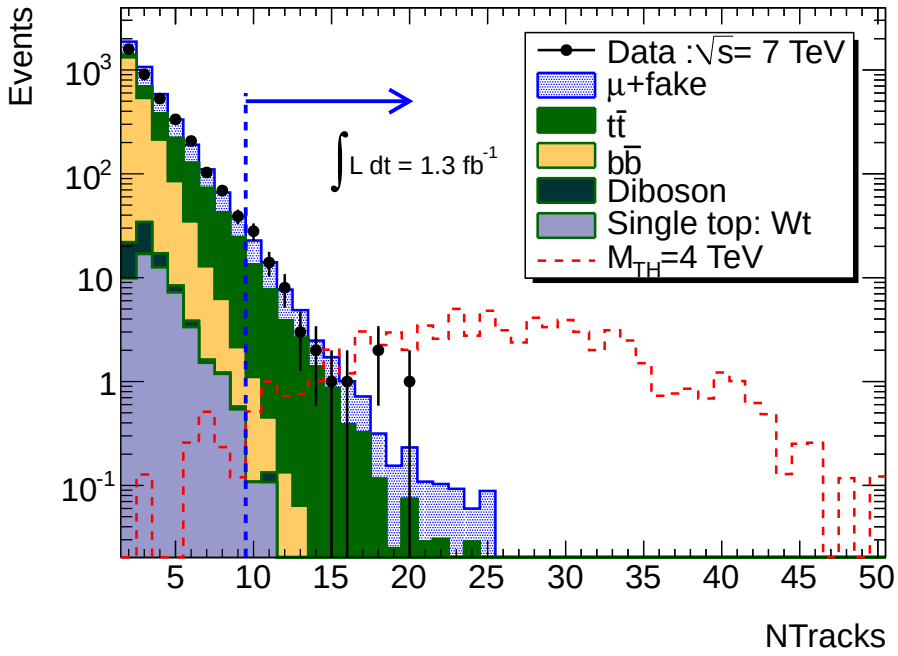

Figure 12: The NTracks distribution for all like-sign dimuon events. In this figure the shape of the $b\bar{b}$ background is taken from the fit shown in Fig. 6. We select the region with NTracks $\geq$ 10 as the signal region. The background histograms are stacked, the signal histogram is overlaid.

Process	Events
$b\bar{b}$	0.77 ± 0.77(syst)
$t\bar{t}$	29.2 ± 0.4(stat) ± 4.1(syst) ± 1.1(lumi)
μ+fake	25.6± 0.3(stat) ± 5.2(syst)
Other backgrounds	0.25 ± 0.11(stat)
Predicted	55.8 ± 0.5(stat) ± 6.8(syst) ± 1.1(lumi)
Observed	60
Signal M_{TH} = 4000 GeV	72.1 ± 2.7(stat) ± 3.6(syst)

Table 6: Number of expected and observed events in the signal region, like-sign dimuon events with NTracks $\geq$ 10. The signal expectation for the point with M_{TH} = 4000 GeV is also shown. The other backgrounds are from diboson and single-top Wt processes.

Process	Events($\mu^+\mu^+$)	Events($\mu^-\mu^-$)
$t\bar{t}$	14.2	15
μ+fake	14	11.6
$\Sigma(t\bar{t}$+fake)	28.2	26.6
Observed	28	32

Table 7: Number of expected and observed events in the signal region broken down by charge of the muons.

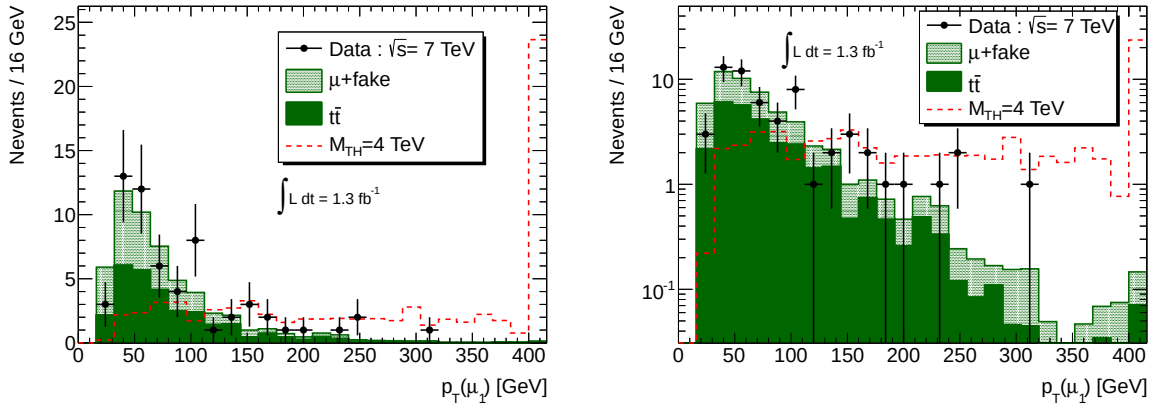

(a) signal region, leading muon p_{T}

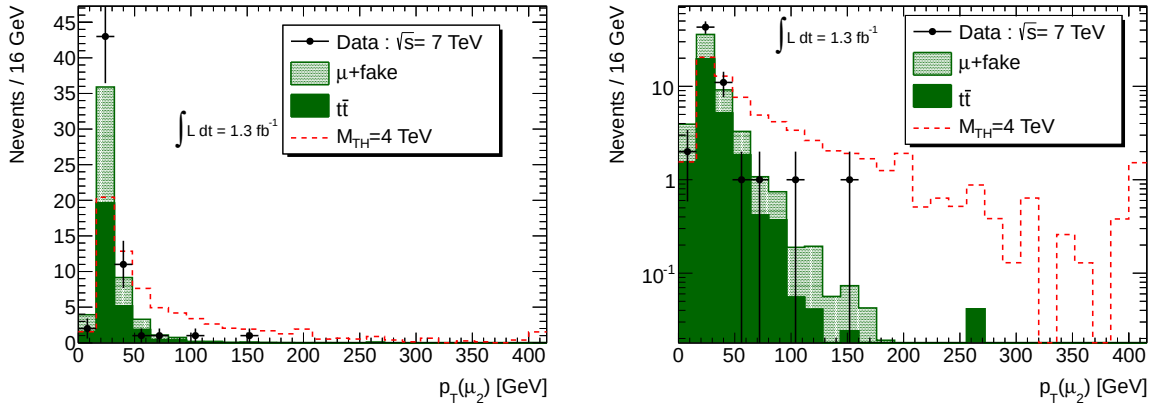

(b) signal region, second muon p_{T}

Figure 13: The leading and second muon p_{T} distributions in the signal region. The background histograms are stacked, the signal histogram is overlaid. The rightmost bin along X-axis shows the overflows.

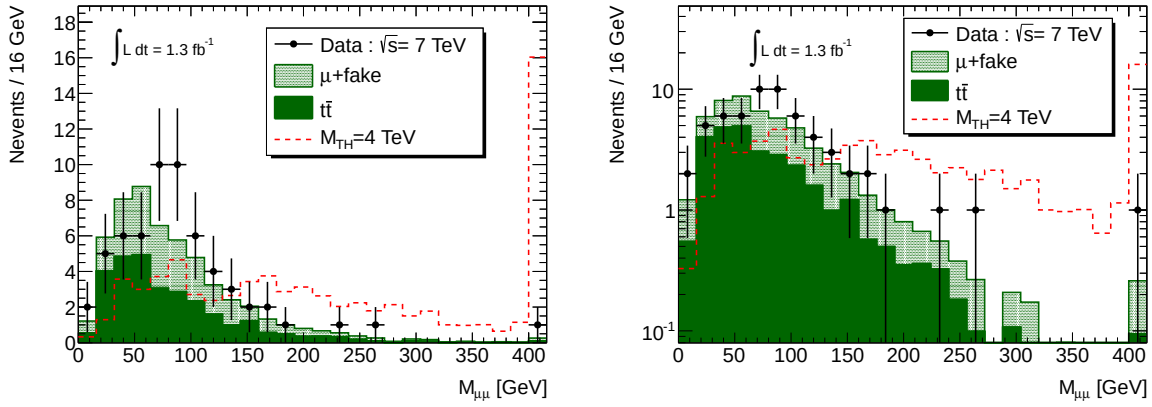

Figure 14: Figure shows the invariant mass distribution of the dimuons in the signal region. The background histograms are stacked, the signal histogram is overlaid. The rightmost bin along X-axis shows the overflows.

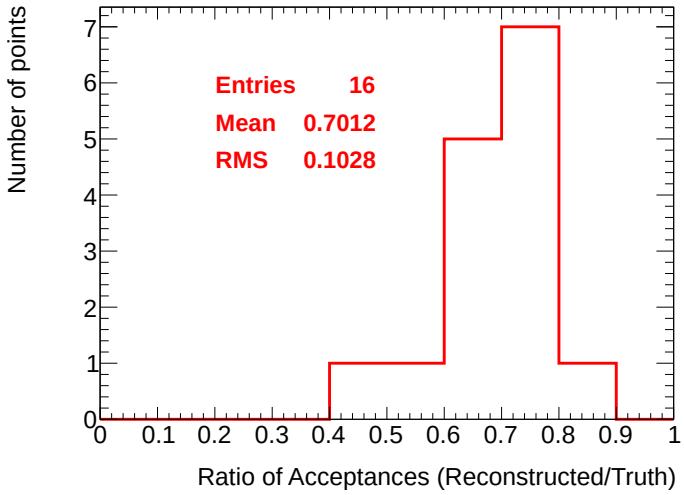

Figure 15: The ratio of reconstructed acceptance to truth acceptance is shown for a subset of the black hole samples.

8 Interpretation of Results

No excess over the predicted standard model background is observed in the signal region. The p-value for the observed result is 0.4 which corresponds to a 0.3 σ excess[4]. Using the observed number of data events and the background expectations, upper limits are set on the cross section (σ) $\times$ the branching ratio to dimuons (BR) $\times$ the acceptance (A) of non standard model contribution in the signal region. The recommended CLs method [34, 35] is used to derive these upper limits. All statistical and systematic uncertainties on the background are taken into account. The observed 95% confidence level limit on $\sigma \times BR \times A$ is 0.018 pb. The observed limit is very close to the expected limit of 0.016 pb. The 1σ and 2σ uncertainty band on the expected limit is 0.012-0.022 and 0.008-0.029 pb respectively.

Limits on the reduced Planck mass ($M_{\rm D}$) and the minimum mass of the black hole ($M_{\rm TH}$) are set for several models. No theoretical uncertainty on signal prediction is assessed, that is, the exclusion limits are set for the exact benchmark models as implemented in the BLACKMAX generator. The observed results are used to obtain exclusion contours in the plane of $M_{\rm D}$ and $M_{\rm TH}$. The $M_{\rm D}$-$M_{\rm TH}$ plane has to be populated by a large number of points to obtain the exclusion contours. For all points in this plane, the signal acceptance is measured using generator level truth information. This truth-level acceptance is compared to the acceptance from full detector simulation for a smaller set of model points (Appendix B : Table 9). To account for the difference in acceptances, the truth level acceptance is scaled by a constant factor of 0.7 ± 0.1 which is measured using the set of fully simulated points. The ratio of reconstructed acceptance to truth accetpance is shown in Fig. 15.

The signal samples are generated with the CTEQ66 PDF. The uncertainty on the signal acceptance from the choice of PDF is estimated by using the 44 error sets of the CTEQ66 PDF. For one signal sample corresponding to a non-rotating black hole in six extra dimensions with $M_{\rm TH}$ = 4000 GeV and $M_{\rm D}$ = 500 GeV, statistically independent samples are generated for each error set. Two sets of such samples are generated, one with 5000 events per sample, and one with 10000 events per sample. Figure 16 (left) shows the acceptance for each sample as a function of error set. The nominal value is at x=0. Acceptances from both sets are shown; in red for 5000 events per sample, in black for 10000 events per sample. The histogram of acceptances from the error sets is shown in Fig. 16 (right). The RMS of the

[4]The p-value is calculated using rs_numbercountingutils.C in Roostats.

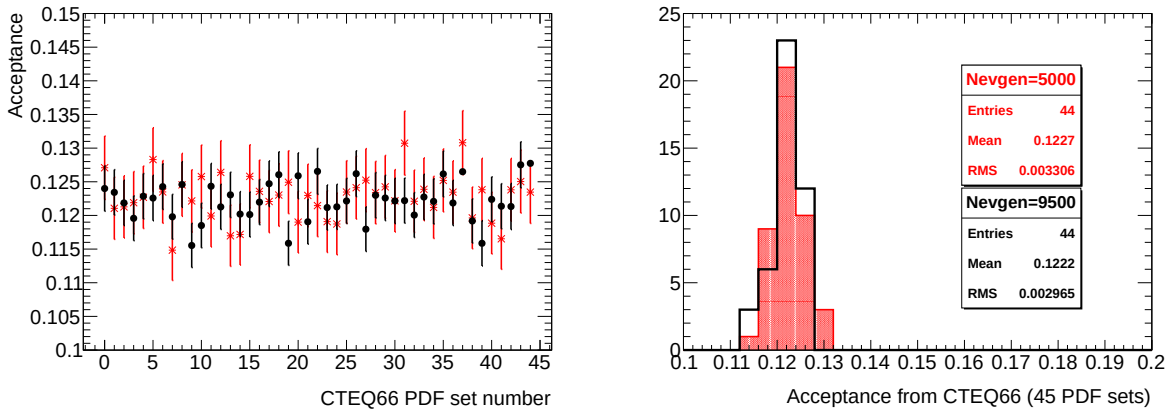

Figure 16: The acceptance from 44 samples corresponding to the error sets of the CTEQ66 PDF set are shown for a signal point with these parameters: $M_{\mathrm{TH}} = 4000\,\mathrm{GeV}$ and $M_{\mathrm{D}} = 500\,\mathrm{GeV}$, $n = 6$, non-rotating black hole. On left, the acceptance is shown for each error set. On right, the histogram of acceptances is shown. In both cases, the red points/curve correspond to 5000 generated events per sample, the black points/curve correspond to 10000 events per sample.

distribution indicates the uncertainty due to signal acceptance. This distribution has been checked for a different signal point as well. The uncertainty is 3% based on these studies.

Thus the uncertainty on the signal prediction consists of the following components: the uncertainty on the truth-level acceptance scaling factor, the uncertainty on signal acceptance due to PDF, the uncertainty on the luminosity of the data sample, the experimental uncertainty on acceptance due to muon trigger and identification measurements and a statistical uncertainty due to the finite MC statistics. These along with the uncertainties on background estimates described previously give the uncertainties on the exclusion limits.

Figure 17 shows the exclusion contours for models with non-rotating and rotating black holes with 2 extra dimensions, while Fig. 18 and 19 shows the exclusion for 4 and 6 extra dimensions respectively. The dashed blue line shows the expected exclusion contour with the 1 σ and 2 σ uncertainty in green and yellow respectively. The solid black line shows the observed exclusion contour. The region below the curves is excluded. The figures also show lines of constant slope ($M_{\mathrm{D}}/M_{\mathrm{TH}}$) of 3, 4 and 5. The semi-classical approximations used for black hole production and decay are only valid for slopes much larger than 1.

9 Conclusion

A search for mini black holes in the final state with two same charge muons was presented in this note. No excess over the standard model predictions was observed. These results are used to exclude models in the (M_D, M_{TH}) plane.

References

[1] N. Arkani-Hamed, S. Dimopoulos, and G. R. Dvali, *The hierarchy problem and new dimensions at a millimeter*, Phys. Lett. **B429** (1998) 263–272, arXiv:hep-ph/9803315.

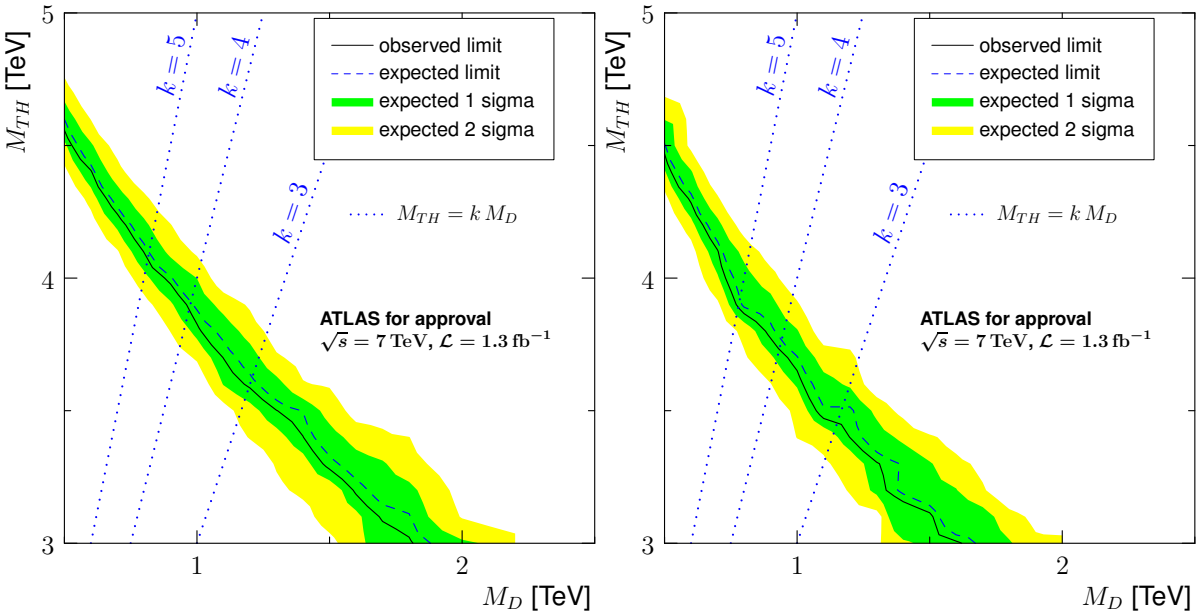

Figure 17: 95% confidence level exclusion contours for non-rotating (left) and rotating (right) black holes with two extra dimensions taking into account all statistical and systematic uncertainties. The dashed blue line shows the expected exclusion contour with the 1 and 2 σ uncertainty in green and yellow respectively. The solid black line shows the observed exclusion contour. The region below the contour has been excluded by this analysis. The figures show lines of constant slope equal to 3,4, and 5. Only slopes much larger than 1 correspond to physical models.

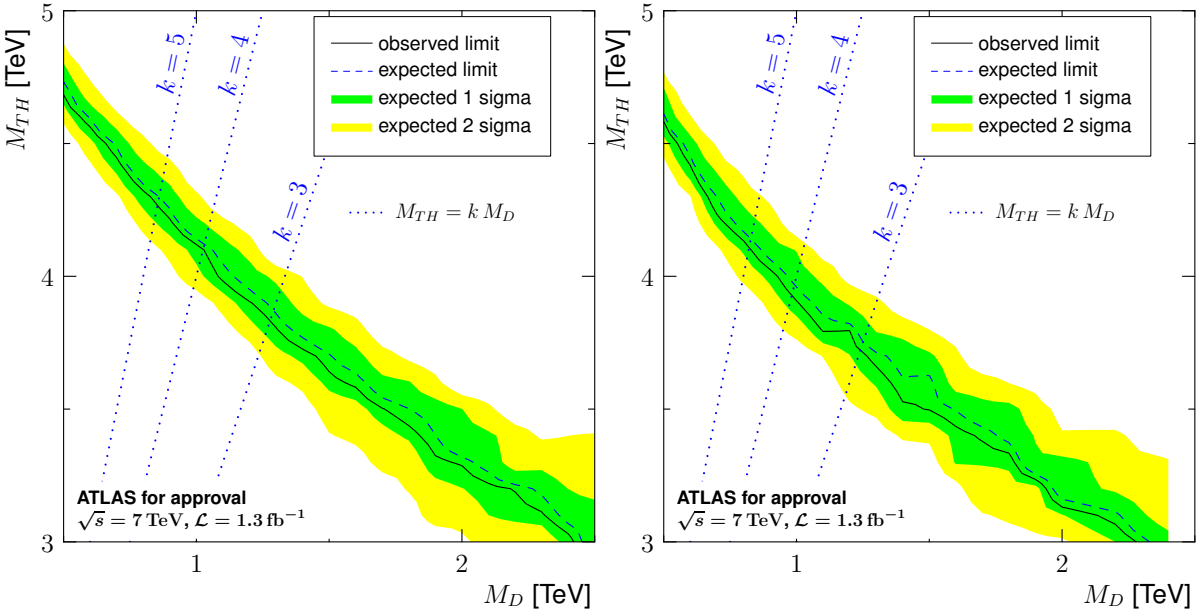

Figure 18: 95% confidence level exclusion contours for non-rotating (left) and rotating (right) black holes with four extra dimensions taking into account all statistical and systematic uncertainties. The dashed blue line shows the expected exclusion contour with the 1 and 2 σ uncertainty in green and yellow respectively. The solid black line shows the observed exclusion contour. The region below the contour has been excluded by this analysis. The figures show lines of constant slope equal to 3,4, and 5. Only slopes much larger than 1 correspond to physical models.

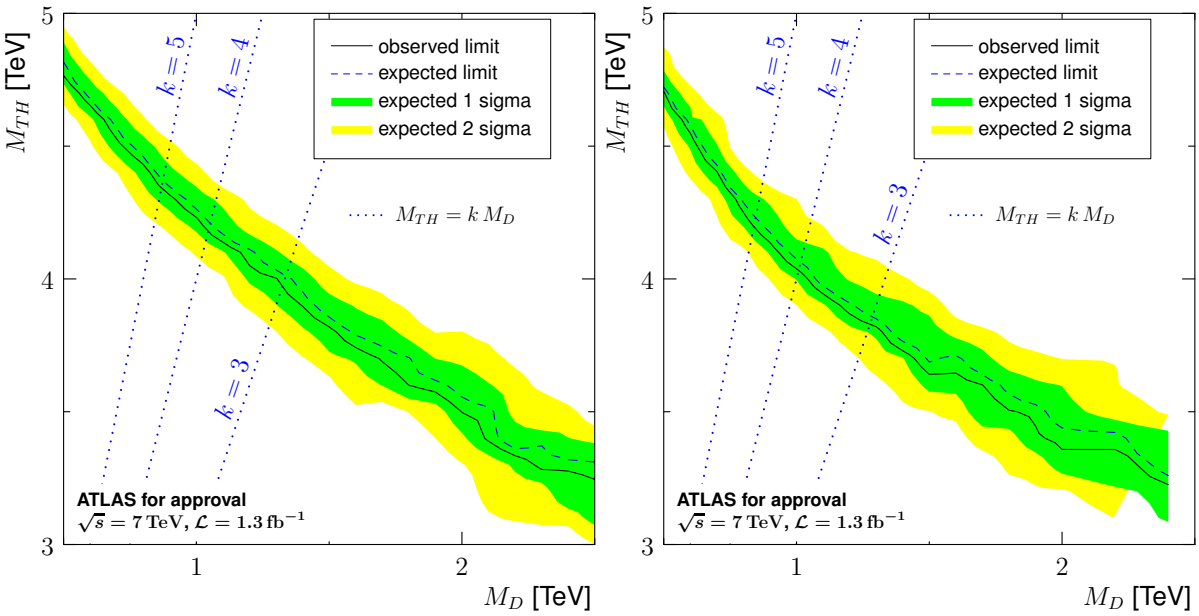

Figure 19: 95% confidence level exclusion contours for non-rotating (left) and rotating (right) black holes with six extra dimensions taking into account all statistical and systematic uncertainties. The dashed blue line shows the expected exclusion contour with the 1 and 2 σ uncertainty in green and yellow respectively. The solid black line shows the observed exclusion contour. The region below the contour has been excluded by this analysis. The figures show lines of constant slope equal to 3,4, and 5. Only slopes much larger than 1 correspond to physical models.

[2] I. Antoniadis, N. Arkani-Hamed, S. Dimopoulos, and G. R. Dvali, *New dimensions at a millimeter to a Fermi and superstrings at a TeV*, Phys. Lett. **B436** (1998) 257–263, arXiv:hep-ph/9804398.

[3] N. Arkani-Hamed, S. Dimopoulos, and G. R. Dvali, *Phenomenology, astrophysics and cosmology of theories with sub-millimeter dimensions and TeV scale quantum gravity*, Phys. Rev. **D59** (1999) 086004, arXiv:hep-ph/9807344.

[4] G. F. Giudice, R. Rattazzi, and J. D. Wells, *Quantum gravity and extra dimensions at high-energy colliders*, Nucl. Phys. **B544** (1999) 3–38, arXiv:hep-ph/9811291.

[5] Particle Data Group Collaboration, K. Nakamura, *Review of particle physics*, J. Phys. **G37** (2010) 075021.

[6] S. Ask, *Search for extra dimensions at LEP*, arXiv:hep-ex/0410004.

[7] CDF Collaboration, T. Aaltonen et al., *Search for large extra dimensions in final states containing one photon or jet and large missing transverse energy produced in $p\bar{p}$ collisions at $\sqrt{s}$ = 1.96-TeV*, Phys. Rev. Lett. **101** (2008) 181602, arXiv:0807.3132 [hep-ex].

[8] D0 Collaboration, V. M. Abazov et al., *Search for large extra dimensions via single photon plus missing energy final states at $\sqrt{s}$ = 1.96-TeV*, Phys. Rev. Lett. **101** (2008) 011601, arXiv:0803.2137 [hep-ex].

[9] CMS Collaboration, V. Khachatryan et al., *Search for Microscopic Black Hole Signatures at the Large Hadron Collider*, Phys. Lett. **B697** (2011) 434–453, arXiv:1012.3375 [hep-ex].

[10] *Search for strong gravity effects in same-sign dimuon final states*, Tech. Rep. ATLAS-CONF-2011-065, CERN, Geneva.

[11] *Search for new physics in like sign dimuon final state*, Tech. Rep. ATL-COM-PHYS-2011-102, CERN, Geneva.

[12] *Search for Mini Black Holes in the Multijet Final State in pp Collisions at* $\sqrt{s}$ = 7 TeV, Tech. Rep. ATL-COM-PHYS-2011-025, CERN, Geneva.

[13] *Search for Microscopic Black Holes in Multi-Jet Final States with the ATLAS Detector at* $\sqrt{s}$ = 7 TeV, Tech. Rep. ATLAS-CONF-2011-068, CERN, Geneva.

[14] *SUSY Group Goodrun Lists*, Available at https://twiki.cern.ch/twiki/bin/view/atlasprotected/luminositysummer2010.

[15] *Updated Luminosity Determination in pp Collisions at root(s)=7 TeV using the ATLAS Detector*, Tech. Rep. ATL-COM-CONF-2011-034, CERN, Geneva.

[16] S. Fixione and B. Webber, *Matching NLO QCD computations and parton shower simulations*, JHEP **06** (2002) 029, arXiv:0204244 [hep-ph].

[17] S. Fixione, P. Nason, and B. Webber, *Matching NLO QCD and parton showers in heavy flavour production*, JHEP **08** (2003) 007, arXiv:0305252 [hep-ph].

[18] J. M. Butterworth et al., *Multiparton interactions in photoproduction at HERA*, Z.Phys.C **72** (1996) 637.

[19] Atlas Collaboration, G. Aad et al., *Measurement of the top quark-pair production cross section with ATLAS in pp collisions at* $\sqrt{s}$ = 7 TeV , accepted by EPJC (2010) , arXiv:1012.1792 [hep-ex].

[20] P. M. Nadolsky, *Implications of CTEQ global analysis for collider observables*, Phys.Rev. **D78** (2008) 031004, arXiv:0802.0007 [hep-ph].

[21] G. Corcella et al., *HERWIG 6.5: an event generator for Hadron Emission Reactions With Interfering Gluons (including supersymmetric processes)*, JHEP **01** (2001) 010, arXiv:0011363 [hep-ph].

[22] B. P. Kersevan and E. Richter-Was, *The Monte Carlo event generator AcerMC version 2.0 with interfaces to PYTHIA 6.2 and HERWIG 6.5*, arXiv:0405247 [hep-ph].

[23] A. Sherstnev and R. S. Thorne, *Parton Distributions for LO Generators*, arXiv:0711.2473 [hep-ph].

[24] D. C. Dai et al., *BlackMax: A black-hole event generator with rotation, recoil, split branes and brane tension*, Phys.Rev. **D77** (2008) 076007, arXiv:0711.3012 [hep-ph].

[25] D. C. Dai et al., *Manual of BlackMax, a black-hole event generator with rotation, recoil, split branes and brane tension*, arXiv:0902.3577 [hep-ph].

[26] *MC10b Production Details*, available at https://twiki.cern.ch/twiki/bin/view/AtlasProtected/AtlasProductionGroupMC10b.

[27] *Observation of t-channel Single Top-Quark Production in pp Collisions at* $\sqrt{s}$ = 7 TeV *with the ATLAS detector*, Tech. Rep. ATLAS-CONF-2011-088, CERN, Geneva.

[28] *Top Group MC10For2011Data*, available at https://twiki.cern.ch/twiki/bin/view/AtlasProtected/TopMC10For2011Data.

[29] *Guidelines for analysis in Rel 15*, available at https://twiki.cern.ch/twiki/bin/view/AtlasProtected/MCPAnalysisGuidelinesRel15.

[30] M. Bianco, E. Gorini, M. Primavera, and A. Ventura, *Efficiencies of Muon Triggers*, Atlas Muon Signature Group weekly meeting 2011-05-26, https://indico.cern.ch/conferenceDisplay.py?confId=140870.

[31] S. Moch and P. Uwer, *Theoretical status and prospects for top-quark pair production at hadron colliders*, Phys. Rev. **D78** (2008) 034003.

[32] U. Langenfeld, S. Moch, and P. Uwer, *New results for $t\bar{t}$ production at hadron colliders, Proc. XVII Int. Workshop on Deep-Inelastic Scattering and Related Topics*, arXiv:0907.2527 [hep-ph].

[33] M. Aliev et al., *HATHOR HAdronic Top and Heavy quarks crOss section calculatoR*, arXiv:1007.1327 [hep-ph].

[34] A. L. Read, *Presentation of search results: The CL(s) technique*, J.Phys. **G28** (2002) 2693–2704.

[35] A. S. Forum, *Frequentist Limits Recommendation*, available at https://twiki.cern.ch/twiki/pub/AtlasProtected/StatisticsTools.

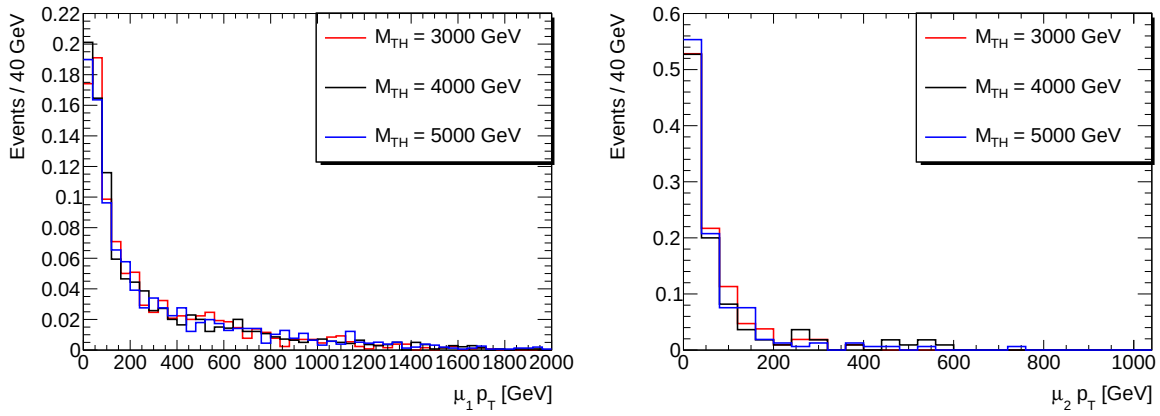

(a) Leading (left) and second (right) muon p_T (linear scale)

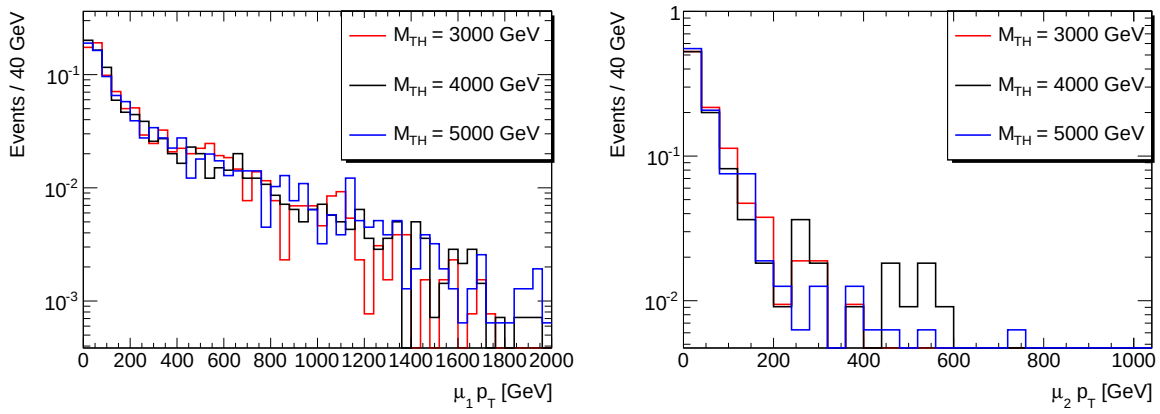

(b) Leading (left) and second (right) muon p_T (log scale)

Figure 20: Figure shows the p_T distribution for leading (left) and second (right) muons for rotating black hole signal in models with 6 extra dimensions. The distributions are shown for three choices of M_{TH}; 3000, 4000, and 5000 GeV with M_D fixed at 1500GeV.

Appendices

A Signal Properties

Figure 20 shows the leading and second muon p_T distributions for three choices of M_{TH} with the other parameters held constant. Figure 21 shows the leading muon isolation distribution for the same choice of models, while Fig. 22 shows the NTracks distribution. None of the distributions except NTracks show strong correlation with M_{TH}.

Figure 23 shows the signal acceptance as function of M_{TH} (left) and M_D (right) with other parameters held constant.

B Details of Monte Carlo samples

Table 8 shows further details of the Monte Carlo samples used in this analysis. Table 9 shows the details of the fully reconstructed signal samples used in Fig. 15.

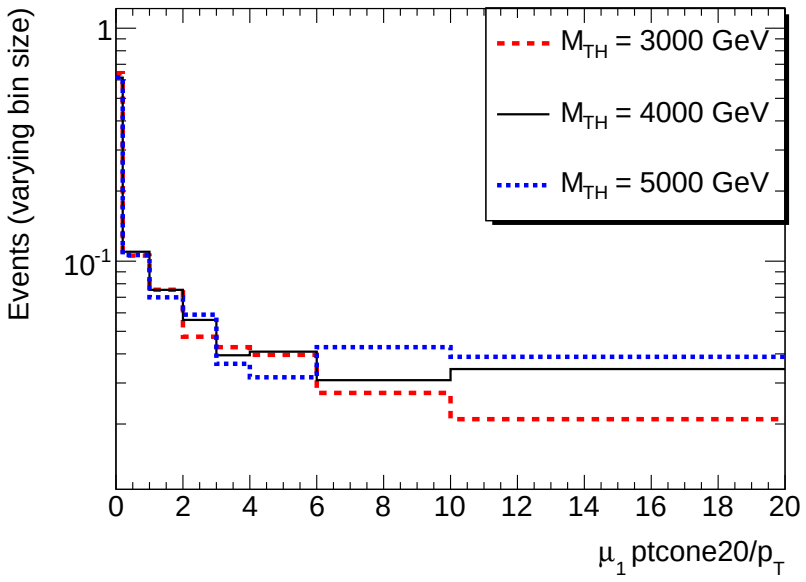

Figure 21: Figure shows the isolation distribution for leading muon for rotating black hole signal in models with 6 extra dimensions. The distributions are shown for three choices of M_{TH}; 3000, 4000, and 5000 GeV with M_{D} fixed at 1500GeV. The first bin corresponds to ptcone20/$p_{\mathrm{T}} < 0.2$ which is the requirement on the leading muon.

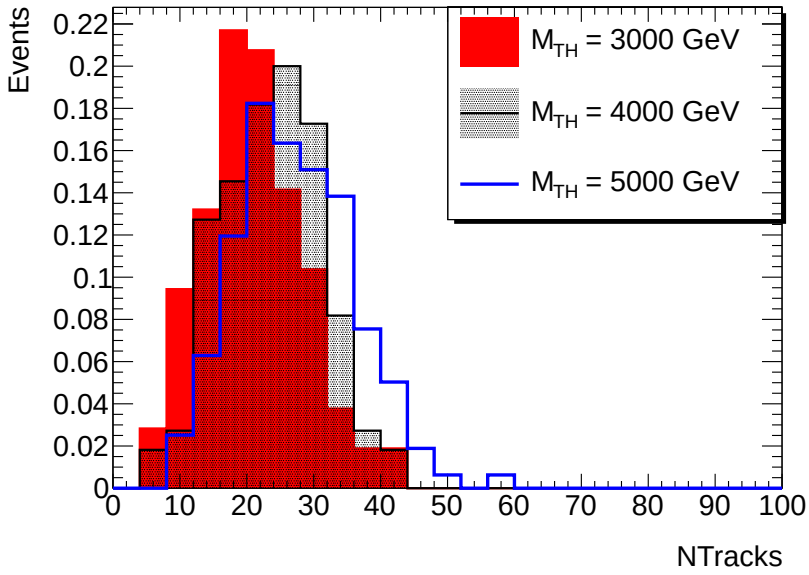

Figure 22: Figure shows the NTracks distribution for rotating black hole signal in models with 6 extra dimensions. The distributions are shown for three choices of M_{TH}; 3000, 4000, and 5000 GeV with M_{D} fixed at 1500GeV.

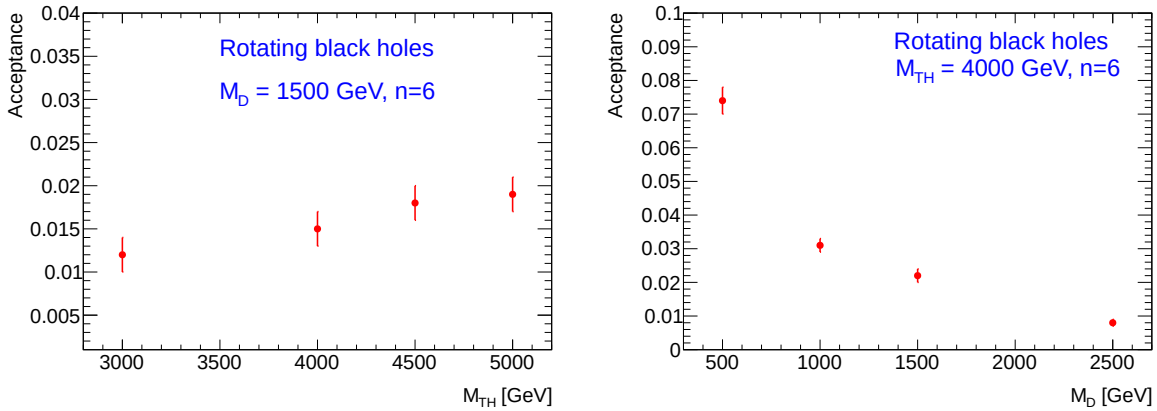

Figure 23: Figure shows the acceptance for a rotating black hole signal in models with 6 extra dimensions. On the left, the acceptance is shown as a function of M_{TH} for fixed M_{D} = 1500 GeV. On the right, the acceptance is shown as a function of M_{D} for fixed M_{TH} = 4000 GeV.

DSN	Process	Cross section	k-factor	filter ϵ	tag
105757	$b\bar{b} + c\bar{c}$	2797			e574_s933_s946_r2302_r2300
105200	$t\bar{t}$	164.6		0.5555	e598_s933_s946_r2302_r2300
105986	ZZ	4.6	1.3	0.21152	e598_s933_s946_r2302_r2300
105987	WZ	11.23	1.6	0.3085	e598_s933_s946_r2302_r2300
105500	Wt	14.6			e703_s933_s946_r2302_r2300
105450	BH	2			e737_s933_s946_r2302_r2300

Table 8: Details of Monte Carlo samples used for background estimates in this analysis. Other black hole samples have also been used as shown in Table 9.

n	M_{TH}	M_{D}	DSN
4	3000	1000	120367
4	3000	1500	120369
4	4000	500	120384
4	4000	1000	120386
4	4500	750	120396
4	5000	1000	120408
6	3000	500	120417
6	3000	1000	120419
6	3000	1500	120421
6	4000	500	120436
6	4000	1000	120438
6	4000	1500	120440
6	4500	750	120448
6	4500	1500	120451
6	5000	1000	120460
6	5000	1500	120462

Table 9: Details of fully reconstructed signal Monte Carlo samples used in this analysis (see Fig. 15).

Sample	LF	LF scaled to 1(fb^{-1})	HF	HF scaled to 1(fb^{-1})
J0	0	0	0	0
J1	0	0	0	0
J2	0	0	1	14635
J3	0	0	35	27365
J4	4	125	153	4792
J5	16	13.4	375	314.7
J6	56	0.7	577	6.92
J7	143	0.01	675	0.066
J8	341	1.5e-6	576	2.5e-6

Table 10: The number of dimuon events from the different jet-jet samples for the nominal selection. LF (HF) designates events where the parent of the leading muon is a light (heavy) flavor meson.

C Fraction of heavy flavor in region *C*

The method to estimate $b\bar{b}$ background as described in Section 5.1 depends on the fraction of heavy flavor to light flavor dimuon events in region C_{data}. Ideally this fraction should be 1. We study the fraction of heavy flavor events for the region *C* selection in simulation. The samples used for this study are the Pythia jet-jet samples (J0 to J8, dataset ID 105009 to 105017 respectively).

For a given dimuon selection, we count the number of dimuon events where the leading muon parent is a heavy flavor meson (400 <pdgID< 600), designated by HF. The dimuon events where the leading muon parent is not from heavy flavor is designated as LF (for light flavor).

In these samples, J0 to J3 have nearly no statistics, but high cross sections as compared to J4 to J8. If all the samples are combined according to respective cross sections, then the J0-J3 samples with large statistical uncertainties dominate the estimates and make drawing any conclusion impossible. To address this we present numbers in two formats. First, we present the individually obtained numbers in each sample, and the simple sum of numbers in each sample. Secondly, we present the cross-section weighted sum of the J5 to J8 samples.

We start with the following nominal selection

- Two muons of the same charge with $p_{\mathrm{T}} > 25, 15$ GeV respectively.
- The leading muon is non isolated; we require ptcone20$/p_{\mathrm{T}} > 0.2$.
- The leading muon has high impact parameter significance; we require $|d_0/d_0^{err}| > 3$.

This gives the fraction of HF to LF as (81 ± 1)% from the simple sum, and (96 ± 1)% from the weighted sum of samples J5-J8. The raw numbers from the different samples are presented in Table 11.

Now in addition to the nominal selection, we require both muons to satisfy $1 - p_{\mathrm{T}}^{MS}/p_{\mathrm{T}}^{ID} < 0.2$, where p_{T}^{MS} and p_{T}^{ID} are the p_{T} of the muon measured in the muon spectrometer (MS) and inner detector (ID) respectively. This distribution is shown in Fig. 24 for all subleading muons in the Alpgen W+jets samples. The distribution is shown separately for muons whose parent is either a light flavor or a heavy flavor meson. After this selection has been imposed, the fraction of HF to LF is (96 ± 1)% from the simple sum, and (98 ± 1)% from the weighted sum of samples J5-J8. The numbers for this heavy flavor enhanced selection are shown in Table 10.

We conclude that after our selections, the fraction of HF in region *C* is very nearly one.

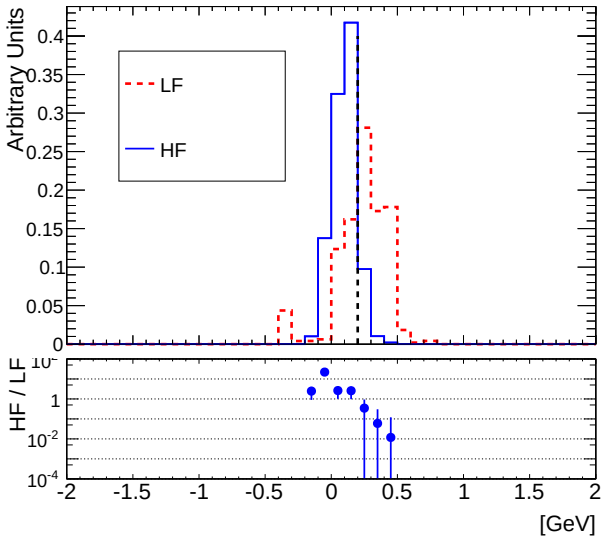

Figure 24: Figure shows the $1 - p_{\mathrm{T}}^{MS}/p_{\mathrm{T}}^{ID}$ distribution for subleading muons in the ALPGEN W+jets samples. LF (HF) designates events where the parent of the subleading muon is a light (heavy) flavor meson. The bottom part of the figure shows the ratio of HF to LF events. We require $1 - p_{\mathrm{T}}^{MS}/p_{\mathrm{T}}^{ID} < 0.2$ in the $b\bar{b}$ control region (region C) to enhance the HF contribution.

Sample	LF	LF scaled to 1(fb^{-1})	HF	HF scaled to 1(fb^{-1})
J0	0	0	0	0
J1	0	0	0	0
J2	0	0	1	14635
J3	0	0	23	17983
J4	4	125	124	3884
J5	5	4.2	269	225.8
J6	7	0.08	368	4.42
J7	19	0.002	337	0.033
J8	17	7.4e-8	182	7.9e-7

Table 11: The number of dimuon events from the different jet-jet samples for the heavy flavor enhanced selection. LF (HF) designates events where the parent of the leading muon is a light (heavy) flavor meson.

Process	Dataset	Generator	Cross section (pb)	Luminosity(pb^{-1})
$W \to \mu\nu$ +0p	107690	ALPGEN	8303.5	417.5
$W \to \mu\nu$ +1p	107691	ALPGEN	1564.8	380.8
$W \to \mu\nu$ +2p	107692	ALPGEN	453.3	8213.3
$W \to \mu\nu$ +3p	107693	ALPGEN	122.3	7928.1
$W \to \mu\nu$ +4p	107694	ALPGEN	30.9	8248.7
$W \to \mu\nu$ +5p	107695	ALPGEN	8.3	8428.7
$W \to \mu\nu$ +jets	119129	SHERPA	10503	161.8
Single-top (t-channel)	108341	MC@NLO	7.12	24928

Table 12: Monte Carlo samples used for fake rate studies described in Appendix D.

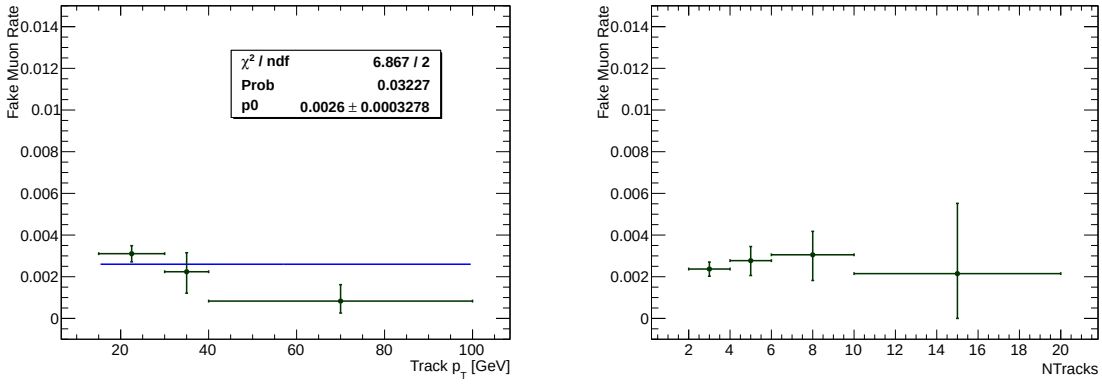

Figure 25: Figure shows the fake rate as measured in the ALPGEN W+jets and single top mixture as a function of track p_{T} on the left, and as a function of NTracks on the right. No dependence is seen on either variable.

D Fake rate studies in MC

The procedure described in Section 5.2 is used to measure the rate of tracks faking muons in the simulated samples. The aim is this study is not to ascertain the absolute scale of the fake rate, but rather to check if the fake rate depends on track p_{T}, or the number of tracks in the event, NTracks.

For this study, we use the W+jets simulated samples. Two sets of samples are considered, one generated with ALPGEN, and the other with SHERPA. To both sets, a single top (t-channel) sample generated with MC@NLO is added. The details of the samples are shown in Table 12.

Figures 25 and 26 show the fake rate as a function of track p_{T} and NTracks. In either case, the fake rate is independent of p_{T} and NTracks.

We also study the composition of the second muon in the ALPGEN samples. The ratio of second ("fake") muons originating from heavy-flavor (b, c meson) decay to pion/kaon decay in flight is roughly one.

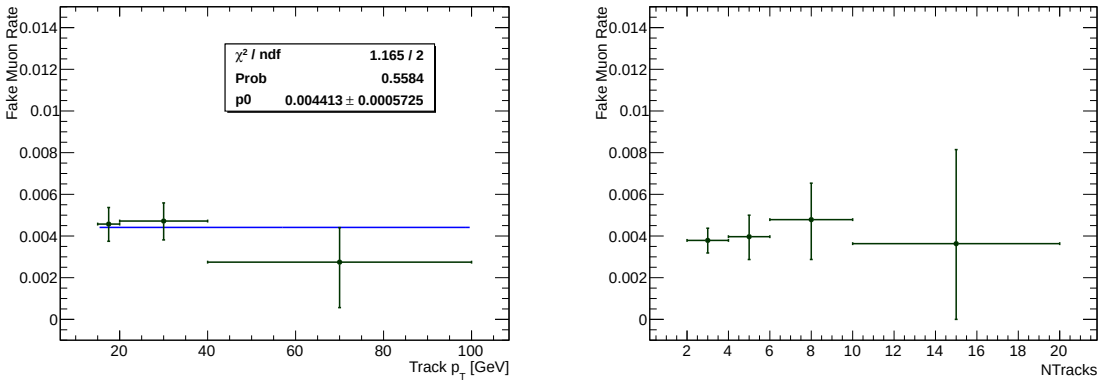

Figure 26: Figure shows the fake rate as measured in the SHERPA W+jets and single top mixture as a function of track p_{T} on the left, and as a function of NTracks on the right. No dependence is seen on either variable.

E Studies of shape of track multiplicity

In Fig. 27, we show the track multiplicity distribution for the different background estimates, and the observed data points. Figure 27 shows the shape of the track multiplicity distributions for the μ+fake, $t\bar{t}$ and $b\bar{b}$ backgrounds. The shape of the μ+fake track multiplicity background is compared to the expected shapes from the W+jet MC samples used in the previous section (Appendix D) in Fig. 28. We can see that the shape of the μ+fake data-driven background agrees well with the expected shapes from MC.

In Fig. 29, we compare the shape of the $t\bar{t}$ track multiplicity distribution using the nominal sample with a $t\bar{t}$ sample generated with POWHEG and hadronized with PYTHIA. The nominal sample is generated with MC@NLO and uses HERWIG+JIMMY for hadronization. The two shapes agree well. The KS probability for the agreement of shapes is 0.99.

In Fig 30, we show the track multiplicity distribution for data and $b\bar{b}$ MC in the the heavy-flavor rich control region defined in Sec. 5.1. The data is normalized to the $b\bar{b}$ MC. The KS probability for the agreement of shapes is 0.96. We repeat the exercise described in Sec. 5.1.2 in this control region. We fit the $b\bar{b}$ MC with an exponential in the range 4 <NTracks< 14. The fit is $e^{6.77-0.48\times\mathrm{NTrack}}$. The fit predicts 2.2 events for NTracks$\geq$ 14, and we observe 1.6 events in the data. The extrapolation procedure is thus verified in the heavy-flavor control region as well.

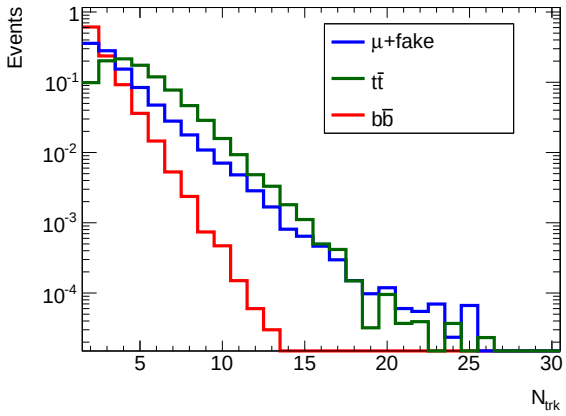

Figure 27: Figure shows the shape of the track multiplicity distribution for the μ+fake, $t\bar{t}$ and $b\bar{b}$ backgrounds.

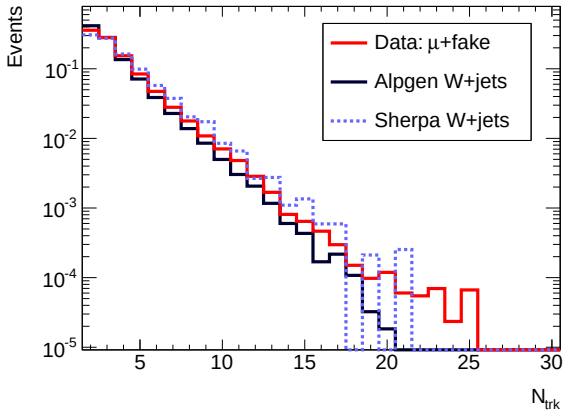

Figure 28: Figure shows the shape of the track multiplicity distribution for the μ+fake data-driven backgrounds compared to the shapes from W+jet MC samples used in Appendix D.

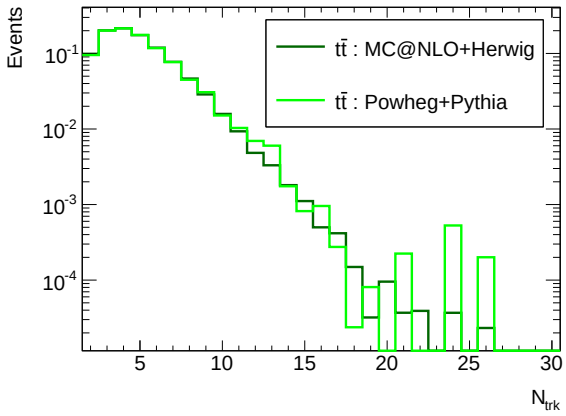

Figure 29: Figure shows the shape of the track multiplicity distribution for the nominal $t\bar{t}$ sample compared to the shapes from a POWHEG + PYTHIA sample. The shapes agree well.

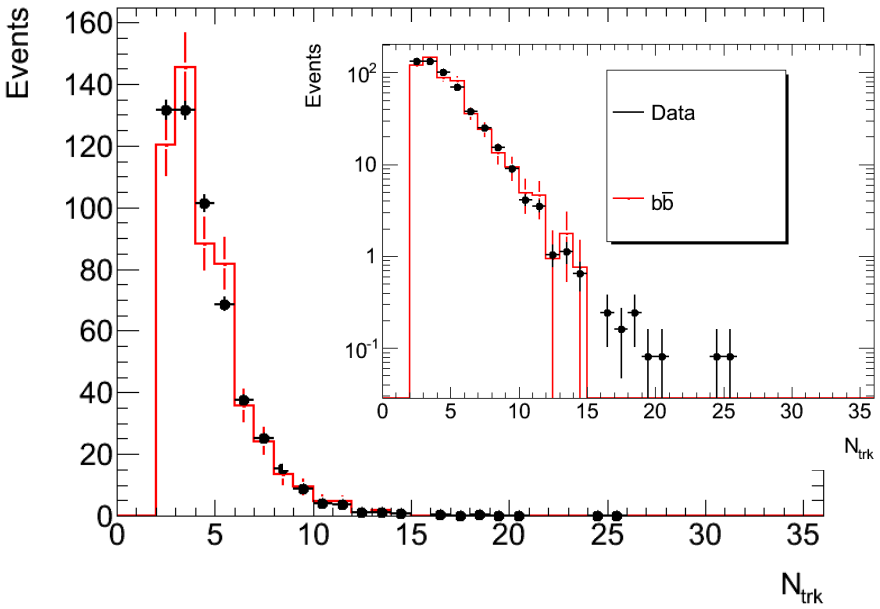

Figure 30: Figure shows the NTracks distribution in linear and log (inset) scales in the heavy-flavor rich control region defined in Sec. 5.1. The data (solid black line) is normalized to the $b\bar{b}$ MC (red points). The KS probability of agreement of shapes is 0.96.

F Fraction of like-sign dimuon events in $b\bar{b}$ Monte-Carlo events with and without mixing

The $b\bar{b}$ Monte-Carlo sample used in this analysis was produced with B meson mixing turned off. In order to estimate the potential effect of this we estimate the fraction of like-sign dimuon pairs expected in a generic sample of $b\bar{b}$ events. The following estimate does not take differences in the $p_{\rm T}$ spectrum of muons B and D decays into account.

We make the following assumptions:

- We consider only muons from B and D decays.
- We assume a single average semi-leptonic branching fraction $f_{SL} = 0.10$ for the decay of all b hadrons and D mesons into a muon (the inclusive branching fractions into muons are quite different for $D^{\pm}$ and D^0, but their average is sufficiently close to 0.10 for the purpose of this estimate).
- We use an average $B - \overline{B}$ mixing parameter $\overline{\chi} = 0.13$ [5].
- We assume the production of at least one D meson in each B decay.
- We define a *right sign muon* as a μ^+ (μ^-) produced directly or through a secondary decay from a $\overline{b}$ (b) hadron. Muons of the opposite charge will be referred to as *wrong sign muons*. Similarly, we refer to D^0, D^+, and D_s^+ ($\overline{D^0}$, D^-, and D_s^-) produced in a $\overline{b}$ (b) hadron decay as *right sign* D since their semi-muonic decay would produce a right sign muon. Based on the inclusive data available from [5]. we assume that a wrong sign D meson is produced in a fraction $w = 0.8$ of

b-hadron decays (a more precise value for w could be obtained from Monte-Carlo, but this didn't seem necessary).

When only muons from B and D decays are considered, we can obtain a like-sign dimuon pair from a generic $b\bar{b}$ event if one of the b-hadrons undergoes mixing or if a wrong sign D decays into a muon. With the above assumptions, the total fraction of like-sign dimuon pairs expected from the different combinations of semi-leptonic decay of b hadron or D meson, mixing, and production of right and wrong sign D mesons is:

$$
\begin{aligned}
f_{pair} = \quad & 2 \cdot f_{SL}^2 \{ \quad (1-\overline{\chi})\overline{\chi} + && (2)\\
& (1-\overline{\chi})(1-f_{SL})\left[(1-\overline{\chi})w + \overline{\chi}(1-w)\right] + && (3)\\
& \overline{\chi}(1-f_{SL})\left[(1-\overline{\chi})(1-w) + \overline{\chi}w\right] + && (4)\\
& (1-f_{SL})^2\left[(1-\overline{\chi})(1-w) + \overline{\chi}w\right] \cdot && (5)\\
& \qquad \left[(1-\overline{\chi})w + \overline{\chi}(1-w)\right] \} && (6)\\
& + O(f_{SL}^3) && (7)
\end{aligned}
$$

Term 1 concerns the case where both muons come from semi-muonic b-hadron decays, terms 2 and 3 are from events where one muon comes from a b-hadron and the other comes from a D decay, while terms 4 and 5 account for muons coming from D decays only. Contributions with more than two semileptonic decays are of $O(f_{SL}^3)$ and are neglected in this simple estimate.

With the numerical values for $\overline{\chi}$ and w indicated above we obtain

$$f_{pair} = 0.87 \cdot 2f_{SL}^2 \tag{8}$$

If mixing is turned off ($\overline{\chi} = 0$), we get

$$f_{pair} = 0.85 \cdot 2f_{SL}^2 \tag{9}$$

Thus with the above assumptions the fractions of like-sign dimuon pairs obtained with and without B mixing are very similar. This is not surprising, given that the fraction w of wrong-sign D mesons is relatively large (i.e. when mixing is turned off, a B meson that would have otherwise decayed after mixing is likely to decay into a wrong-sign D meson and to produce a muon of the required charge, thus compensating for turning off mixing).

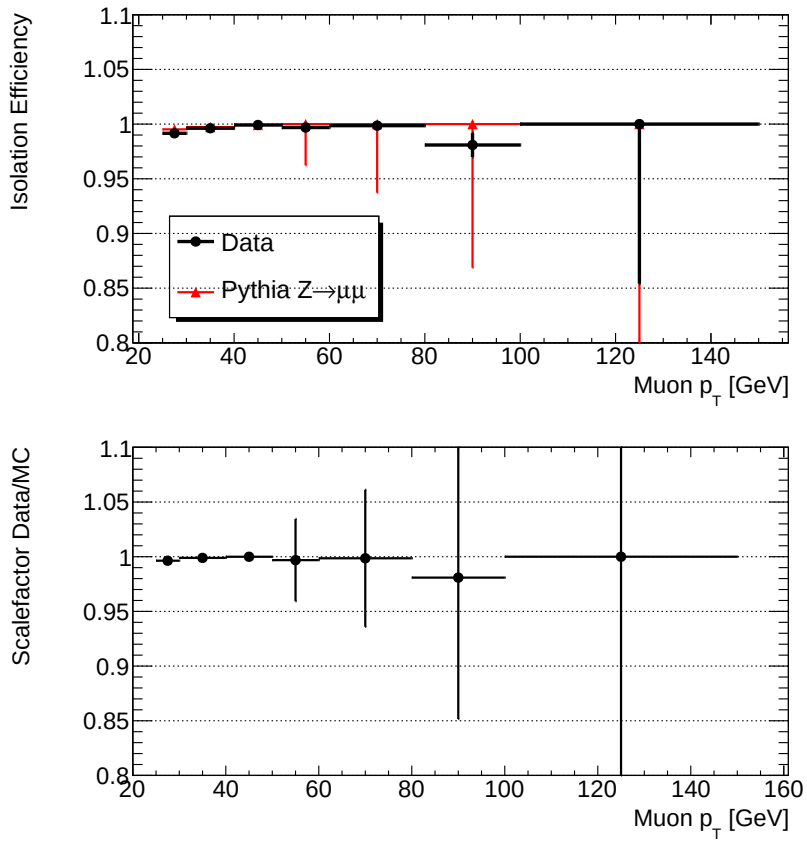

Figure 31: Figure shows the isolation efficiency in data and MC (top) and the scalefactor (Data/MC). The scale factor is 0.999.

G Miscellaneous Studies

In this section, we present other auxiliary studies.

We check the efficiency of our isolation selection, ptcone20/$p_{\mathrm{T}} < 0.2$ in a sample of Z events. We use the standard tag-and-probe method. Events with two muons of opposite sign and with invariant mass satisfying $81 < M_{\mu\mu}(\,\mathrm{GeV}) < 101$ are selected. The muon selection is the same as described for the analysis. The tag muon is required to be isolated, and the efficiency for the probe muon to be isolated is measured in data and MC. The data sample is the same as the one used for this analysis. The MC sample is a Pythia $Z \rightarrow \mu\mu$ sample with MC10b pileup conditions. Figure 31 shows the measured isolation efficiency in data and MC and the scale factor (Data/MC). The measured scale factor is 0.999. We also the measure the scale factor for the d_0 significance requirement ($d_0/d_0^{err} < 3$) for these Z events. The scale factor for isolated probes is 0.998. Both the isolation and d_0 significance scale factors are close to 1 and we do not apply any corrections to the MC samples in this analysis.

We also find that the isolation efficiency in signal is stable at high p_{T}. In Figure 32, we show the isolation efficiency for the leading muon for two different black hole samples. The efficiency is only measured for truly isolated muons by requiring that the muons originate promptly from the black hole, or arise from the decay of W or Z bosons from the black hole.

To check the effect of pileup, we measure the isolation efficiency for muons in the Z, $t\bar{t}$ and $b\bar{b}$ MC samples as a function of $< \mu >$, the average number of interactions per event. Here the efficiency is measured for all muons matched to a truth-level muon. Figure 33 shows that the efficiency for our

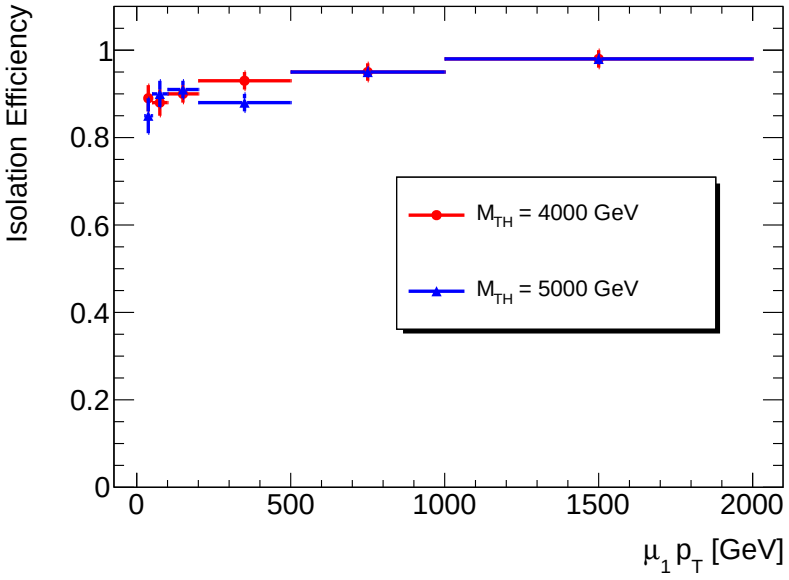

Figure 32: Figure shows the isolation efficiency for leading muon in different signal MC samples as a function of muon p_{T}. The efficiency is measured only for those muons which originate promptly from the black hole, or for muons arising from the decay of W and Z bosons from the black hole.

isolation cut is stable for all $< \mu >$.

We also check to see if our track selection is sensitive to pileup. Figure 34 shows the two dimensional distribution of NTracks versus $< \mu >$ for events with at least two muons with $p_{\mathrm{T}} > 15$ GeV each. We check to see if the NTracks are correlated with the number of interactions; the correlation factors[5] show no such correlation. This is expected since the track p_{T} is required to be greater than 10 GeV and the tracks are required to point back to the same vertex as the muons in the event.

H Miscellaneous Figures

Figure 35 shows the distribution of events in the $b\bar{b}$ and $t\bar{t}$ simulation samples in the different regions as described by Fig. 1. Figures 37, 38, 39, 40, 41, and 42 show the ratio of data to predicted background in the bottom part of the figure; these figures are counterparts to figs. 9, 10, 11, 12, 13, and 14 respectively.

Figures 43,43, and 43 show the limit plots for 2, 4 and 6 extra dimensions respectively with the actual sample points used for limit calculation overlaid as black points.

I Location of code

The code used for this analysis can be found here:
https://svnweb.cern.ch/trac/atlasgrp/browser/Institutes/LBNL/MultiObjectAnalysis

[5] TH2::GetCorrelationFactor()

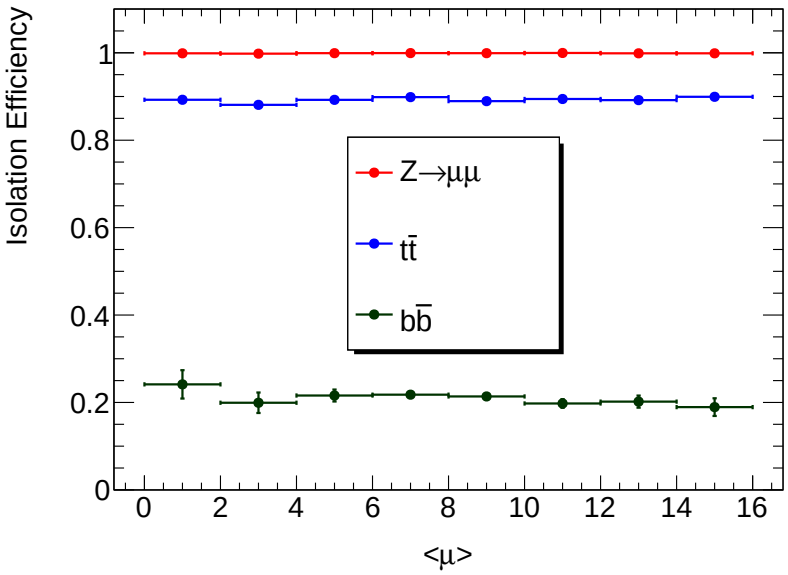

Figure 33: Figure shows the isolation efficiency in different MC samples as a function of $< \mu >$. The efficiency is stable for all $< \mu >$.

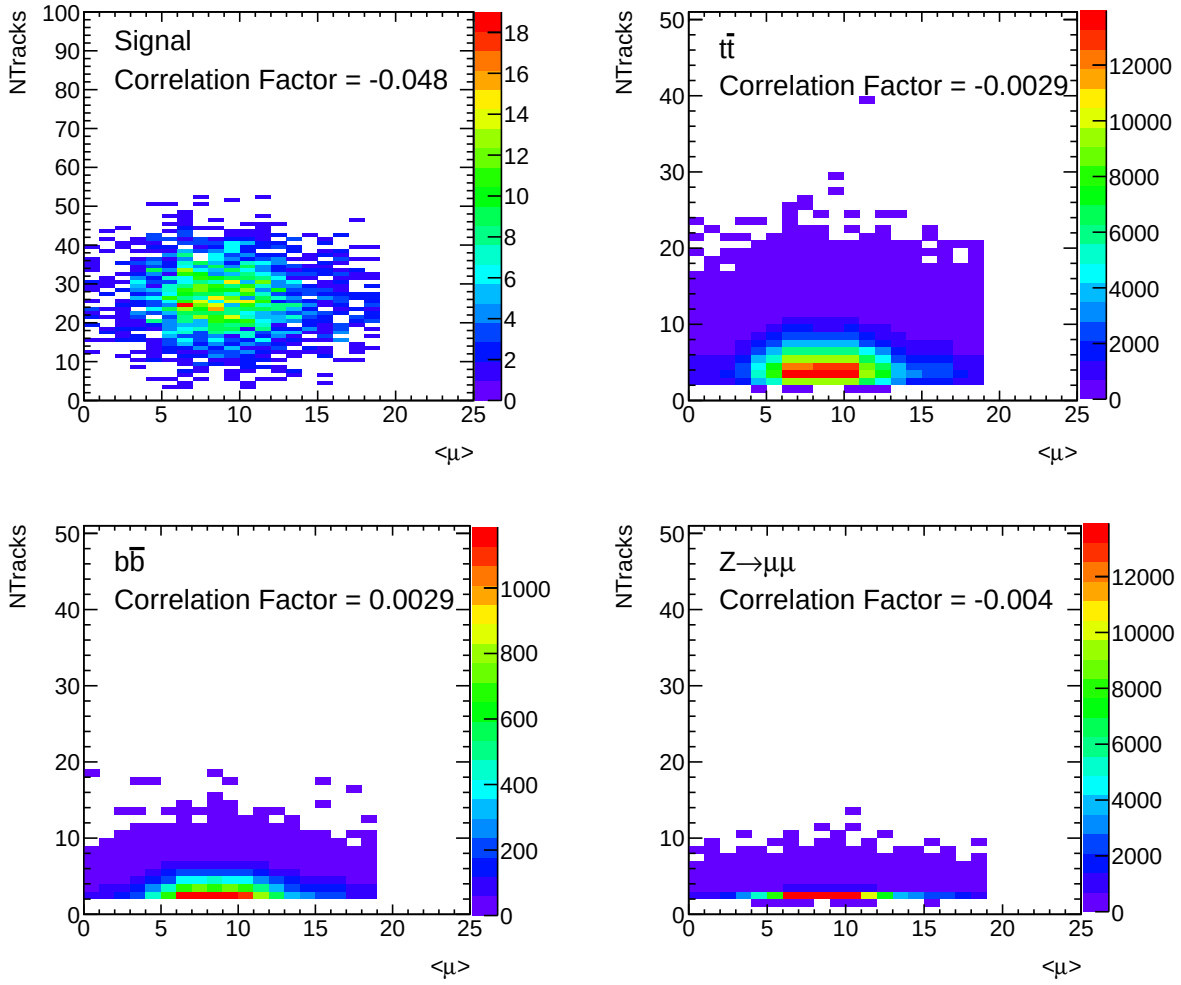

Figure 34: Figure shows the distribution of NTracks versus $< \mu >$ for events with at least two muons with $p_{\mathrm{T}} > 15$ GeV each in different simulation samples. NTracks is found to be uncorrelated with $< \mu >$ as indicated by the correlation factors shown in the figure.

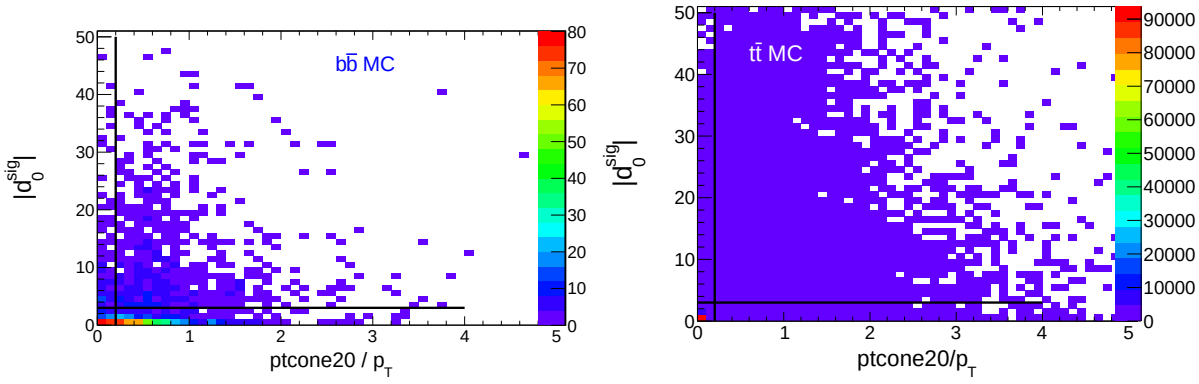

Figure 35: Figure shows the regions as described in Fig. 1 populated by events for the $b\bar{b}$ MC (left) and for the $t\bar{t}$ MC (right).

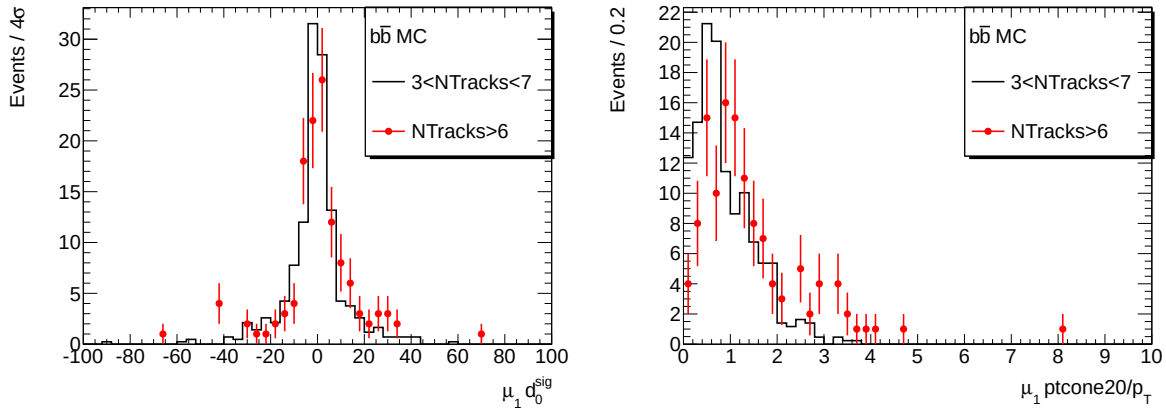

Figure 36: Figure shows the d_0/d_0^{err} (left) and relative isolation (right) distributions for the leading muon for all dimuon events in the $b\bar{b}$ MC for events with 3 <NTracks< 7 and NTracks> 6. The distributions are normalized to area. The KS probability of agreement of shapes is 0.66 for d_0 significance and 6.6×10^{-4} for the isolation.

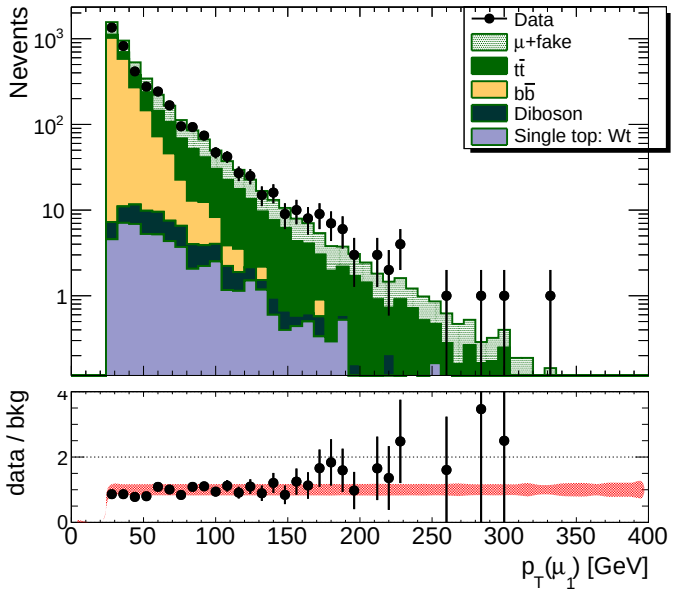

Figure 37: The leading muon p_{T} distribution in log scale in the background region (NTracks < 10). The background histograms are stacked. The bottom part of the figure shows the ratio of data to prediction. The error on the points is statistical, while the red band shows the systematic uncertainty.

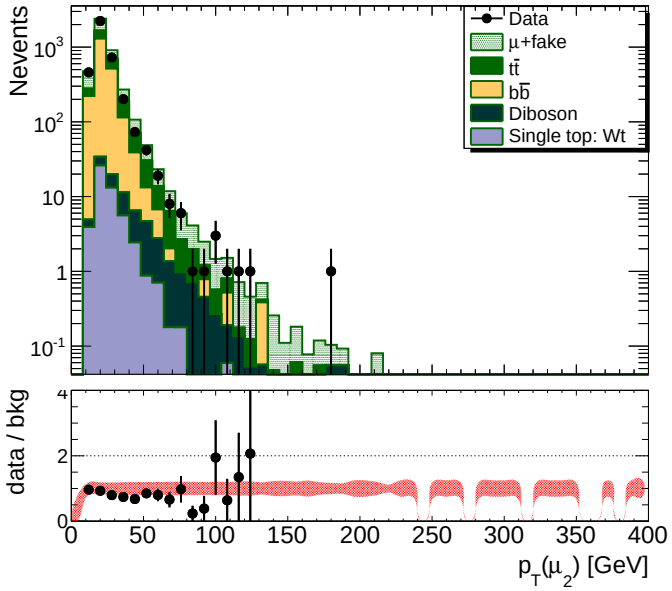

Figure 38: The second muon p_{T} distribution in log scale in the background region (NTracks < 10). The background histograms are stacked. The bottom part of the figure shows the ratio of data to prediction.The error on the points is statistical, while the red band shows the systematic uncertainty.

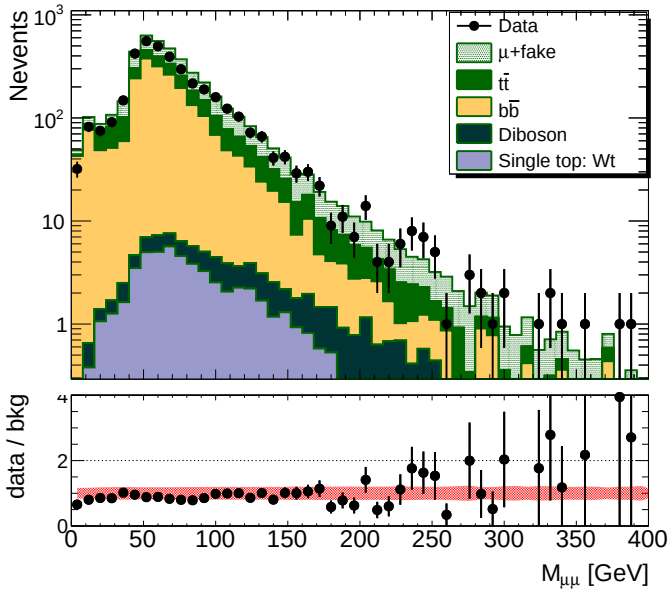

Figure 39: The invariant mass distribution of the two muons in log scale in the background region (NTracks < 10). The background histograms are stacked. The bottom part of the figure shows the ratio of data to prediction. The error on the points is statistical, while the red band shows the systematic uncertainty.

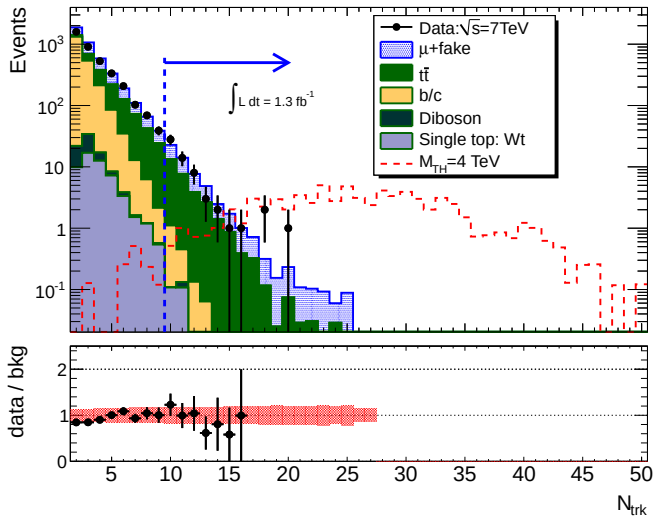

Figure 40: The NTracks distribution for all like-sign dimuon events. In this figure the shape of the $b\bar{b}$ background is taken from the fit shown in Fig. 6. The background histograms are stacked, the signal histogram is overlaid. The bottom part of the figure shows the ratio of data to prediction. The error on the points is statistical, while the red band shows the systematic uncertainty.

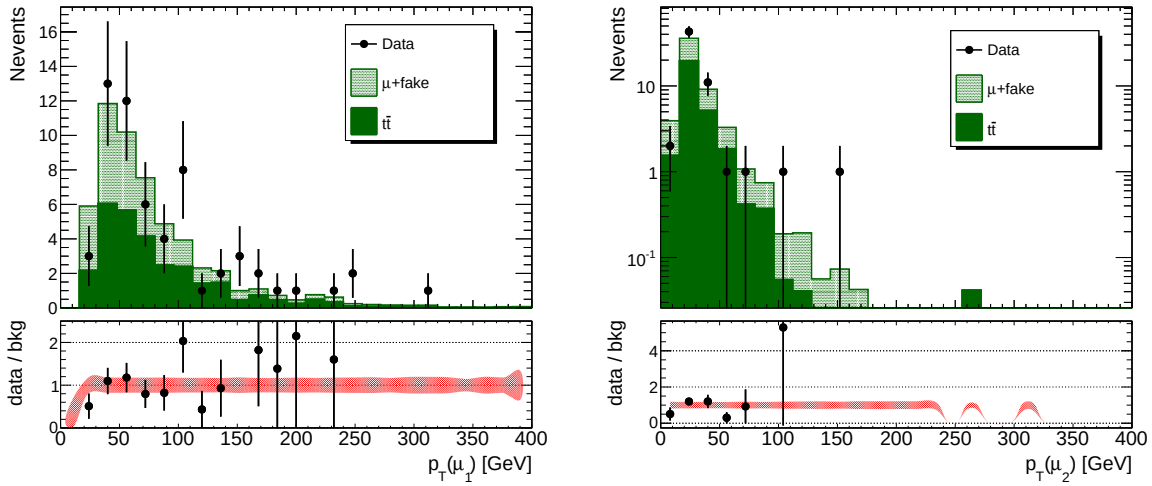

Figure 41: The leading (left) and second (right) muon p_{T} distributions in the signal region. The background histograms are stacked, the signal histogram is overlaid. The bottom part of the figure shows the ratio of data to prediction. The error on the points is statistical, while the red band shows the systematic uncertainty.

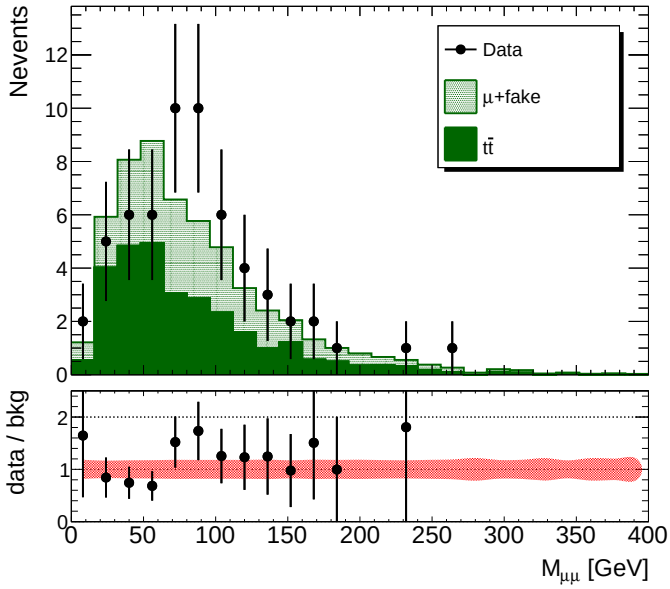

Figure 42: Figure shows the invariant mass distribution of the dimuons in the signal region. The background histograms are stacked, the signal histogram is overlaid. The bottom part of the figure shows the ratio of data to prediction. The error on the points is statistical, while the red band shows the systematic uncertainty.

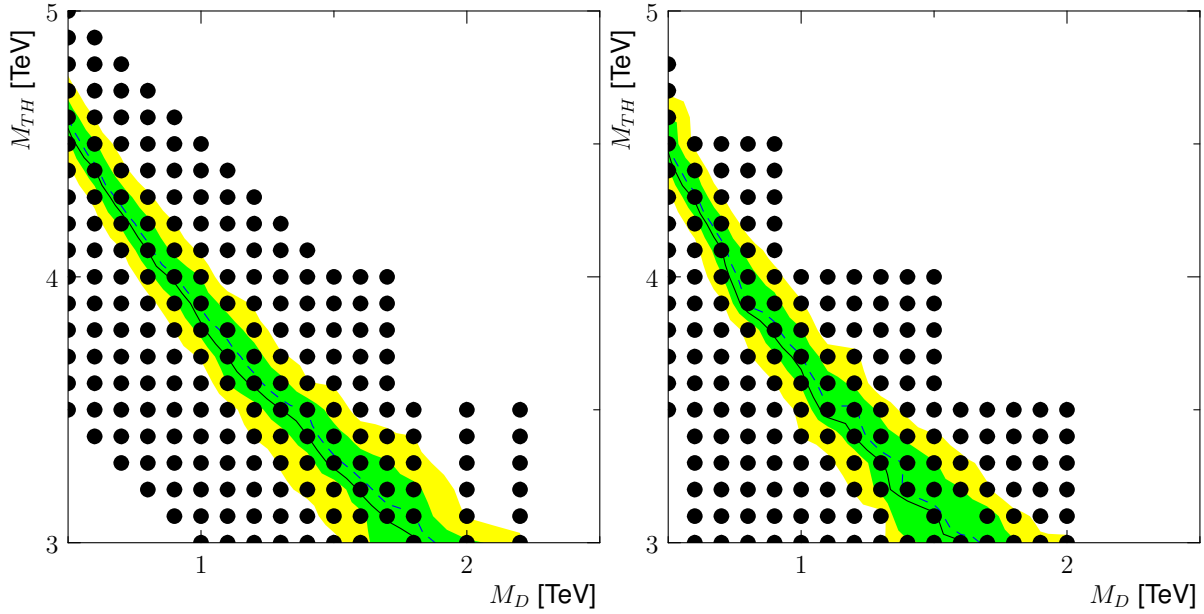

Figure 43: 95% confidence level exclusion contours for non-rotating (left) and rotating (right) black holes with two extra dimensions taking into account all statistical and systematic uncertainties. The dashed blue line shows the expected exclusion contour with the 1 and 2 σ uncertainty in green and yellow respectively. The solid black line shows the observed exclusion contour. The region below the contour has been excluded by this analysis. The figures show lines of constant slope equal to 3,4, and 5. Only slopes much larger than 1 correspond to physical models. The actual sample points used for the limit calculation are shown as black dots.

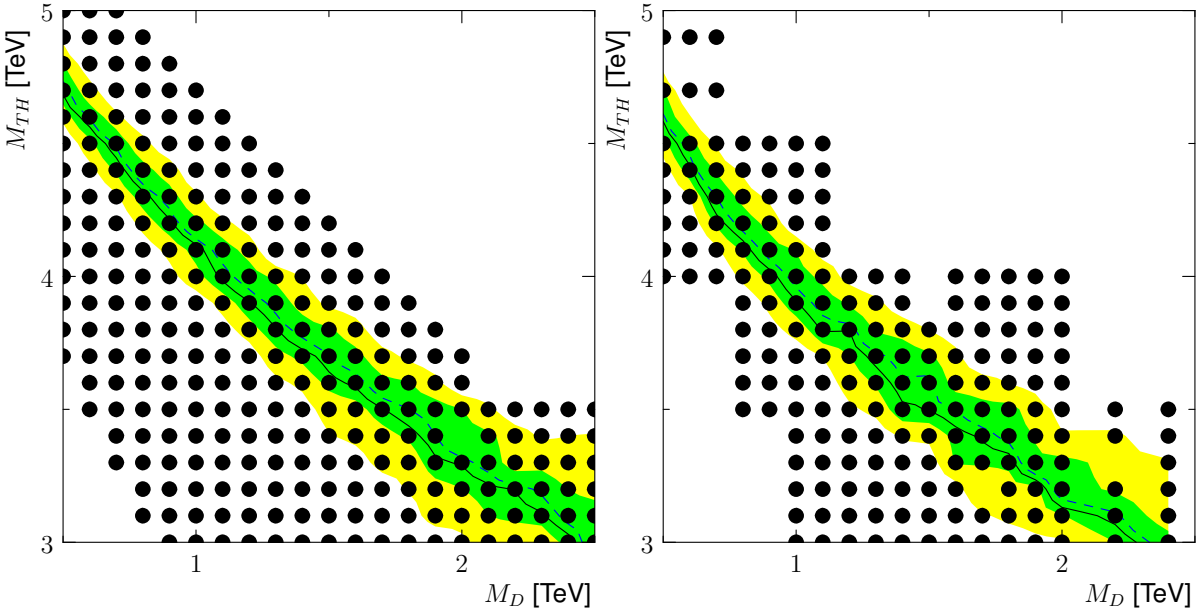

Figure 44: 95% confidence level exclusion contours for non-rotating (left) and rotating (right) black holes with four extra dimensions taking into account all statistical and systematic uncertainties. The dashed blue line shows the expected exclusion contour with the 1 and 2 σ uncertainty in green and yellow respectively. The solid black line shows the observed exclusion contour. The region below the contour has been excluded by this analysis. The figures show lines of constant slope equal to 3,4, and 5. Only slopes much larger than 1 correspond to physical models. The actual sample points used for the limit calculation are shown as black dots.

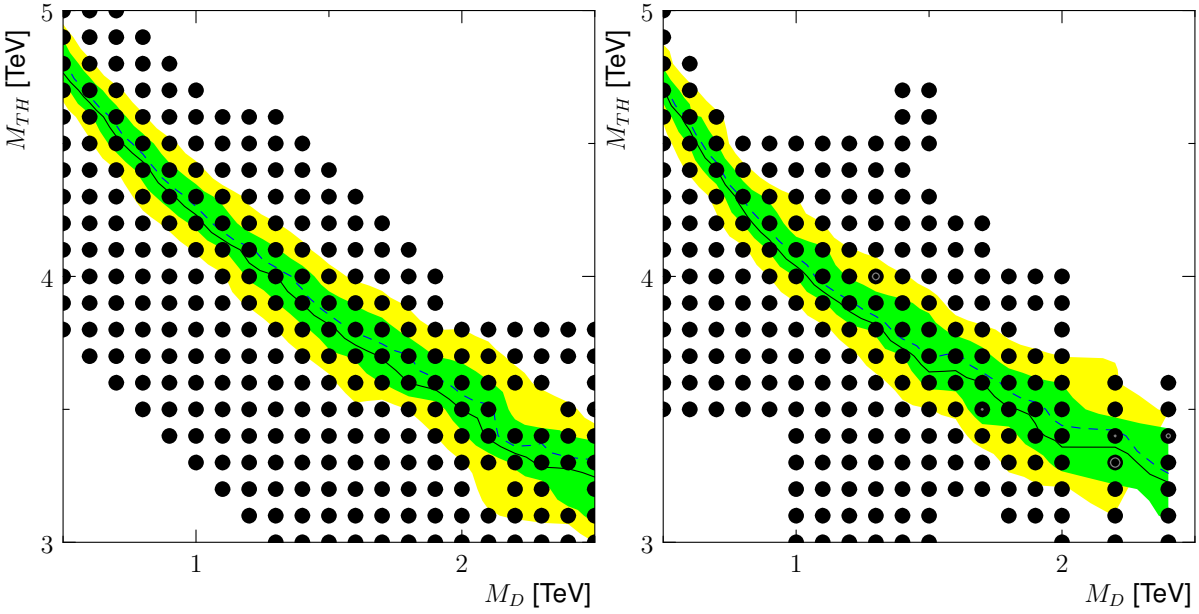

Figure 45: 95% confidence level exclusion contours for non-rotating (left) and rotating (right) black holes with six extra dimensions taking into account all statistical and systematic uncertainties. The dashed blue line shows the expected exclusion contour with the 1 and 2 σ uncertainty in green and yellow respectively. The solid black line shows the observed exclusion contour. The region below the contour has been excluded by this analysis. The figures show lines of constant slope equal to 3,4, and 5. Only slopes much larger than 1 correspond to physical models. The actual sample points used for the limit calculation are shown as black dots.